CHAPTER 11

The plume mode

Mantle plumes are buoyant mantle upwellings that are inferred to exist under some volcanic centres. In Chapter 8 I stated the basic idea that convection is driven by thermal boundary layers that become unstable, detach from the boundary and thereby drive flow in the interior of a fluid layer. In Chapter 10 we looked at plates as a thermal boundary layer of the convecting mantle, driving a distinctive form of convection in the mantle that I called the *plate mode* of mantle convection.

Here we look at the evidence that there is a mode of mantle convection driven by a lower, hot thermal boundary layer, at the expected form of such a mode, and at the consistency of the evidence with that expectation. Since it will become clear that the form and dynamics of such upwellings, or plumes, are quite different from the downwellings of lithosphere driving the plate mode, I will call the plumes and the flow they drive the *plume mode* of mantle convection.

11.1 Volcanic hotspots and hotspot swells

In Chapter 3 I described Wilson's observation that there are, scattered about the earth's surface, about 40 isolated volcanic centres that do not seem to be associated with plates and that seem to remain fixed relative to each other as plates move around (Figure 11.1). Their fixity (or at least their slow motion relative to plate velocities) is inferred from the existence of 'hotspot tracks', that is of chains of volcanoes that are progressively older the further they are from the active volcanic centre. Wilson was building on the inferences of Darwin and Dana that a number of the island chains in the Pacific seem to age progressively along the chain.

The classic example is the Hawaiian volcanic chain of islands and seamounts, evident in the topography shown in Figure 11.2.

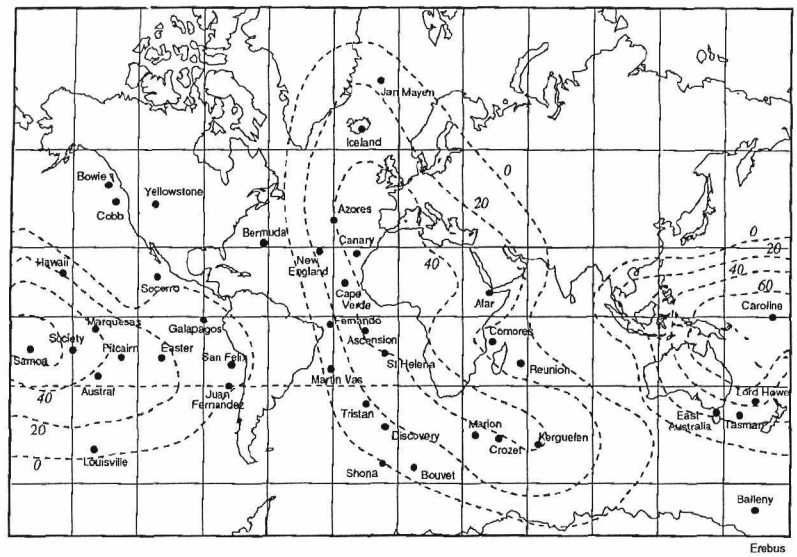

Figure 11.1. Locations of volcanic hotspots (dots). Residual geoid contours (in m) are superimposed (from Crough and Jurdy [1]). The residual geoid may reflect mainly signal from the lower mantle. Hotspots correlate with residual geoid highs but not with the present plate boundaries. From Duncan and Richards [2]. Copyright by the American Geophysical Union.

The south-eastern extremity of this chain, the island of Hawaii, is volcanically active, and the islands and seamounts to the north-west are progressively older. Wilson [3] hypothesised that the source of the eruptions was a 'mantle hotspot' located in a region of the mantle where convective velocities are small, such as the middle of a convection 'cell'. Morgan [4, 5] proposed instead that the source of the eruptions is a mantle plume, that is a column of hot, buoyant mantle rising from the core–mantle boundary.

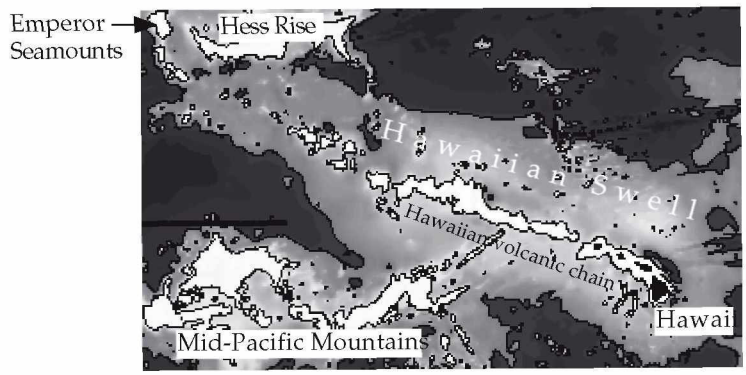

Figure 11.2. Topography of the sea floor near the Hawaiian Islands, showing the volcanic chain of islands and seamounts and the broad swell surrounding them. The contours are at depths of 3800 m and 5400 m.

Wilson's hypothesis had the disadvantages that the existence of the mantle hotspot was *ad hoc*, with no obvious reason for being there, and that it was not clear how a finite volume of warmer mantle could provide a steady supply of volcanism for tens of millions of years. Morgan's hypothesis at least implied a plausible physical source and the potential for longevity. Morgan's hypothesis immediately became the preferred one. Because of this, I proposed, in Chapter 3, dropping the concept of an internal mantle hotspot, and using the term 'volcanic hotspot' for the surface expression of the mantle phenomenon.

The number of volcanic hotspots has been variously estimated between about 40 [1, 6] and over 100 [7], but it is debatable whether many of the latter might be associated with individual mantle plumes. Figure 11.1 shows 40 hotspot locations selected by Duncan and Richards [2]. Contours of the hydrostatic geoid (i.e. relative to the shape of a rotating hydrostatic earth) are included. The suggestion is that hotspots correlate with highs in the geoid, which plausibly are due to structure in the lower mantle (Chapter 10), and specifically to regions of the deep mantle that are warmer because there has been no subduction into them in the past 200 Ma or so [8]. On the other hand, it is striking that hotspots show little correlation with the present configuration of plate boundaries.

As well as the narrow topography of the Hawaiian volcanic chain, there is evident in Figure 11.2 a broad swell in the sea floor surrounding the chain. This swell is up to about 1 km high and about 1000 km wide. Such a swell might be due to thickened oceanic crust, to a local imbalance of isostasy maintained by the strength of the lithosphere, or to buoyant material raising the lithosphere. Seismic reflection profiles show that the oceanic crust is not significantly thicker than normal [9]. Nor can such a broad swell be held up by the flexural strength of the lithosphere. The colder parts of the lithosphere behave elastically even on geological time scales, as long as their yield stress is not exceeded. For lithosphere of the age of that near Hawaii, about 90 Ma, the effective elastic thickness of the lithosphere is about 30 km thick, and it has a flexural wavelength of about 500 km [10]. However the wavelength of the swell is about 2000 km. If the swell were held out of isostatic balance by the lithosphere, the stresses would exceed the plausible yield stress of the lithosphere.

The straightforward conclusion is that the Hawaiian swell is held up by buoyant material under the lithosphere. In conjunction with the existence of the isolated volcanic centre, it is then a straightforward inference that there is a narrow column of hot mantle rising under Hawaii. Both the unusual volcanism and the

supply of buoyancy to the base of the lithosphere would be explained if the column had a higher temperature than normal mantle. The volcanism occurs in a small, isolated locality far from plate boundaries, in contrast, for example, to the curvilinear volcanic island arcs near subduction zones. The isolation implies that the buoyant material is in the form of a column rather than a sheet. Since the active volcanism is confined to within an area of the order of 100 km across, it is reasonable to infer that the column diametre is of the same order. The fact that the Hawaiian hotspot track extends, through the bend into the Emperor seamounts, to ages of at least 90 Ma indicates that the mantle source is long-lived, and not due to an isolated heterogeneity within the mantle. Morgan called such a hot, narrow column a *mantle plume*.

11.2 Heat transported by plumes

Swells like that in Figure 11.2 are evident around many of the identified volcanic hotspots. Other conspicuous examples are at Iceland, which straddles the Mid-Atlantic Ridge, and at Cape Verde, off the west coast of Africa (Figure 4.3). The latter is 2 km high and even broader than the Hawaiian swell, presumably because the African plate is nearly stationary relative to the hotspot [2].

The swells can be used to estimate the rate of flow of buoyancy in the plumes. Buoyancy, as we saw in Chapter 8, is the gravitational force due to the density deficit of the buoyant material. If the plume is envisaged as a vertical cylinder with radius r and if the plume material flows upward with an average velocity u (as in Figure 7.7), then the buoyancy flow rate is

$$b = g\Delta\rho \cdot \pi r^2 u \tag{11.2.1}$$

where $\Delta\rho = (\rho_p - \rho_m)$ is the density difference between the plume and the surrounding mantle.

The way buoyancy flow rate can be inferred from hotspot swells is clearest in the case of Hawaii. The Hawaiian situation is sketched in Figure 11.3, which shows a map view and two cross-sections. As the Pacific plate moves over the rising plume column it is lifted by the plume buoyancy. There will be a close isostatic balance between the weight of the excess topography created by this uplift and the buoyancy of the plume material under the plate, as we discussed in Section 8.8. Since the plate is moving over the plume, the parts of the plate that are already elevated are being carried away from the plume. In order for the swell to persist, new

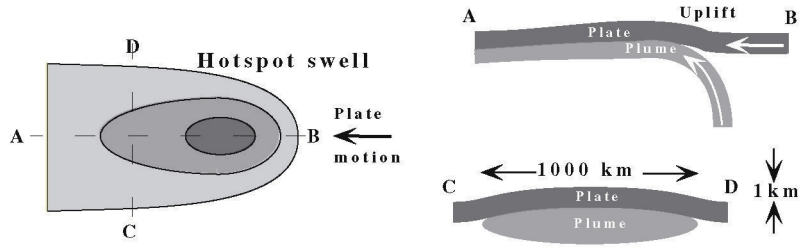

Figure 11.3. Sketch of a hotspot swell like that of Hawaii (Figure 11.2) in map view (left) and two cross-sections, showing the relationship of the swell to the plume that is inferred to be below the lithosphere. The swell is inferred to be raised by the buoyancy of the plume material. This allows the rate of flow of buoyancy and heat in the plume to be estimated.

parts of the plate have to be continuously raised as they arrive near the plume. This requires the arrival of new buoyant plume material under the plate (cross-section AB). Thus the rate at which new swell topography is generated will be a measure of the rate at which buoyant plume material arrives under the lithosphere.

The addition to swell topography each year is equivalent to elevating by a height $h = 1\,\text{km}$ a strip of sea floor with a 'width' $w = 1000\,\text{km}$ (the width of the swell) and a 'length' $v\delta t = 100\,\text{mm}$ (the distance travelled by the Pacific plate over the plume in one year at velocity $v = 100\,\text{mm/a}$). Both the sea floor and the Moho are raised, and sea water is displaced, so the effective difference in density is that between the mantle (ρ_m) and sea water (ρ_w). The rate of addition to the weight (negative buoyancy) of the new swell is then

$$W = g(\rho_\text{m} - \rho_\text{w})wvh = b \tag{11.2.2}$$

By the argument just given, the buoyancy flow rate b in the plume is equal to W. Using the values quoted above yields $b = 7 \times 10^4\,\text{N/s}$ for Hawaii.

If the plume buoyancy is thermal, it can be related to the rate of heat transport by the plume, since both depend on the excess temperature, $\Delta T = T_\text{p} - T_\text{m}$, of the plume. Thus the difference between the plume density, ρ_p, and the mantle density is

$$\rho_\text{p} - \rho_\text{m} = \rho_\text{m}\alpha\Delta T \tag{11.2.3}$$

while the heat flow rate is (see Section 7.7)

$$Q = \pi r^2 u \rho_\text{m} C_P \Delta T \tag{11.2.4}$$

Taking the ratio of Q and b and using Equation (11.2.3) then yields

$$Q = C_P b/g\alpha \tag{11.2.5}$$

Note particularly that this relationship does not depend on the excess temperature of the plume. In fact this is the same relationship as we derived in Section 10.4.4 between the buoyancy and heat flow rates of plates (Equation (10.4.4)). Thus this is another specific and quantitative example of the general relationship between convection and topography that we discussed in Section 8.8.

With $C_P = 1000\,\text{J/kg}\,^\circ\text{C}$ and $\alpha = 3 \times 10^{-5}/^\circ\text{C}$ this yields roughly $Q = 2 \times 10^{11}\,\text{W}$, which is about 0.5% of the global heat flow. The total rate of heat transport by all known plumes has been estimated very roughly by Davies [11], and more carefully by Sleep [12], with similar results. Although there are 40 or more identified hotspots, all of them are weaker than Hawaii and many of them are substantially weaker. The total heat flow rate of plumes is about $2.3 \times 10^{12}\,\text{W}$ (2.3 TW), which is about 6% of the global heat flow (41 TW, Table 10.1).

This value is comparable to estimates of the heat flow out of the core. Stacey [13] estimated this from the thermal conductivity of the core and its adiabatic temperature gradient, obtaining 3.7 TW for the heat that would be conducted down this gradient. Convective heat transport in the core would add to this, but compositional convection, due to continuing solidification of the inner core, might subtract from it. Another estimate can be made from thermal history calculations (Chapter 14), in which the core cools by several hundred degrees through earth history. Taking the present cooling rate to be about $70\,^\circ\text{C/Ga}$, the core mass to be $1.94 \times 10^{20}\,\text{kg}$ and the specific heat to be $500\,\text{J/kg}\,^\circ\text{C}$ yields a rate of heat loss of about 2.3 TW.

These estimates carry substantial uncertainty. As well, the estimate of plume heat flow rate should include the heat carried by plume heads (Sections 11.4, 11.5). Hill *et al.* [14] used the frequency of flood basalt eruptions in the geological record of the past 250 Ma to estimate that plume heads carry approximately 50% of the heat carried by plume tails. Thus the total heat flow rate in plumes would be approximately 3.5 TW, less than 10% of the global heat flow rate.

The approximate correspondence of the estimate of the heat transported by plumes with the rate of heat loss from the core supports Morgan's proposal that plumes come from a thermal boundary layer at the base of the mantle. According to our general discussion of convection in Chapter 8, a bottom thermal boundary

layer is formed when heat enters through the bottom boundary of a fluid layer.

Stacey and Loper [15] were apparently the first to appreciate that this implies that plumes are cooling the core, in the sense that they are the agent by which heat from the core is mixed into the mantle. In this interpretation, the role of plumes is primarily to transfer heat from the core *through* the mantle, but not *out of* the mantle. Plumes bring heat to the base of the lithosphere, which is mostly quite thick and conducts heat only very slowly to the surface. For example, no excess heat flux has been consistently detected over the Hawaiian swell [16]. While in some cases, like Iceland, the lithosphere is thin and a substantial part of the excess plume heat may be lost to the surface, more commonly much of the plume heat would remain in the mantle, presumably to be mixed into the mantle after the overlying lithosphere subducts.

11.3 Volume flow rates and eruption rates of plumes

It was stressed above that the buoyancy flow rate of a plume can be estimated from the swell size without knowing the plume temperature. However, if we do have an estimate of plume temperature it is then possible to estimate the volumetric flow rate of the plume. It is instructive to compare this with the rate of volcanic eruption.

From the petrology of erupted lavas, plumes are estimated to have a peak temperature of 250–300 °C above that of normal mantle [17]. The volumetric flow rate up the plume is $\Phi_p = \pi r^2 u$, where u is the average velocity in the conduit and r is its radius. From Equations (11.2.1) and (11.2.3), this is related to the buoyancy flow rate, b, by

$$\Phi_p = b/g\rho_m\alpha\Delta T \tag{11.3.1}$$

b was also related to the rate at which the swell volume is created, $\Phi_s = wvh$, through the weight of topography, W, in Equation (11.2.2):

$$\Phi_s = wvh = W/g(\rho_m - \rho_w) = b/g(\rho_m - \rho_w) \tag{11.3.2}$$

so the plume volumetric flow rate is related to the swell volumetric rate of creation through

$$\Phi_p = \Phi_s(\rho_m - \rho_w)/\rho_m\alpha\Delta T \tag{11.3.3}$$

For example, for Hawaii $\Phi_s = 0.1\,km^3/a$. If $\rho_m = 3300\,kg/m^3$, $\rho_w = 1000\,kg/m^3$, $\alpha = 3 \times 10^{-5}/°C$ and $\Delta T = 300\,°C$, then $(\rho_m - \rho_w)/\rho_m \alpha \Delta T = 75$. In other words the plume volumetric flow rate is about 75 times the rate of uplift of the swell. Thus for Hawaii $\Phi_p = 7.5\,km^3/a$.

The Hawaiian eruption rate, that is the rate at which the volcanic chain has been constructed, has been about $\Phi_e = 0.03\,km^3/a$ over the past 25 Ma [18, 19]. It is immediately evident that this is very much less than the plume volumetric flow rate. It implies that only about 0.4% of the volume of the plume material is erupted as magma at the surface. Even if there is substantially more magma emplaced below the surface, such as at the base of the crust under Hawaii [9, 20], the average melt fraction of the plume is unlikely to be much more than 1%.

Since the magmas show evidence of being derived from perhaps 5–10% partial melting of the source [17, 21], this presumably means that about 80–90% of the plume material does not melt at all, and the remainder undergoes about 5–10% partial melt. This result is important for the geochemical interpretation of plume-derived magmas and it is also useful for evaluating an alternative hypothesis for the existence of hotspot swells (Section 11.6.3).

11.4 The dynamics and form of mantle plumes

Having looked at the observational evidence for the existence of mantle plumes, and having derived some important measures of them, we now turn to the fluid dynamics of buoyant upwellings. Our understanding of the physics of such upwellings is quite well-developed, and there are some inferences and predictions that can be made with considerable confidence. This means that the hypothesis of mantle plumes can potentially be subjected to a number of quantitative observational tests.

This understanding of plume dynamics has arisen from some mathematical results, some long-standing and some more recent, and from some elegant laboratory experiments supplemented by physical scaling analyses and some numerical modelling. Plume dynamics is more tractable than plate dynamics largely because plumes are entirely fluid.

11.4.1 Experimental forms

The buoyant upwellings from a hot thermal boundary layer might have the form of sheets or columns. The downwellings driven by sinking plates clearly have the form of sheets, at least in the upper

part of the mantle, since plates are stiff sheets at the surface and subduct along continuous curvilinear trenches. The stiffness of the plate would be expected to preserve this form to some depth, and recent results of seismic tomography seem to confirm this expectation (Chapter 5).

In contrast, Whitehead and Luther [22] showed experimentally and mathematically that upwellings from a buoyant fluid layer preferentially form columns rather than sheets. In experiments starting with a thin uniform fluid layer underlying a thick layer of a more dense fluid, the less dense fluid formed upwellings that started as isolated domes, rather than as sheets. Whitehead and Luther supplemented this laboratory demonstration with a mathematical analysis of second-order perturbation theory that showed that the rate of growth of a columnar upwelling is greater than the rate of growth of a sheet upwelling. This is an extension of the Rayleigh–Taylor instability that we encountered in Section 8.4.

Whitehead and Luther's experiments also demonstrated that the viscosity of an upwelling relative to the viscosity of the fluid it rises through has a strong influence on the form of the upwelling. This is illustrated in Figure 11.4, which shows buoyant upwellings

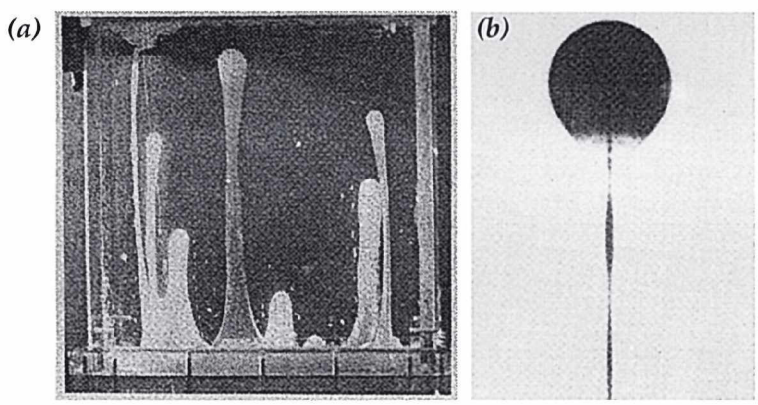

Figure 11.4. Photographs from laboratory experiments showing the effect of viscosity on the forms of buoyant upwellings. (a) The buoyant fluid is more viscous than the fluid it rises through, and the upwellings have fairly uniform diameter. In this case the buoyant fluid began as a thin uniform layer at the base of the tank. From Whitehead and Luther [22]. Copyright by the American Geophysical Union. (b) The buoyant fluid is less viscous than the fluid it rises through, and the upwelling has the form of a large spherical head and a thin columnar tail. In this case the buoyant fluid was injected through the base of the tank, and dyed to distinguish it. From Richards, Duncan and Courtillot [23]. Copyright American Association for the Advancement of Science. Reprinted with permission.

rising from the base of a tank. If the buoyant fluid is much more viscous than the ambient fluid (Figure 11.4a), the diameter of the buoyant columns is fairly uniform over its height. If the buoyant fluid is much less viscous (Figure 11.4b), then the column has a large, nearly spherical head at the top with a very thin conduit or tail connecting it to source. The reason for these different forms can be understood fairly simply, and this will be addressed in the next section.

Each of the experiments shown in Figure 11.4 involved two different fluids with different densities and viscosities. However, in the mantle we expect that the material ascending in a plume is the same material as normal mantle, but hotter. The higher temperature would make the plume less dense, and also lower its viscosity (Section 6.10.2). We might expect therefore that a mantle upwelling from a hot thermal boundary layer would form a plume, and that the plume would have a head-and-tail structure, as in Figure 11.4b. This is confirmed by the experiment illustrated in Figure 11.5a which shows a plume formed by heating a fluid whose viscosity is a strong function of temperature. The viscosity of the plume fluid is about 0.3% of the viscosity of the surrounding fluid, and the plume has a pronounced head-and-tail structure.

A striking new feature in Figure 11.5a is that the injected fluid forms a spiral inside the plume head. This is caused by thermal entrainment of surrounding, clear fluid into the head. As the head rises, heat diffuses out of it into the surrounding, cooler fluid, forming a thermal boundary layer around the head. Because this fluid is heated, it becomes buoyant, and so it tends to rise with the head. The spiral structure forms because there is a circulation within the plume head, with an upflow in the centre, where hot new fluid is arriving from the conduit, and a relative downflow around the equator, where the rise of the plume is resisted by the surrounding fluid. The fluid from the thermal boundary layer around the head is entrained into this internal circulation, flowing up next to the central conduit. This process is quantified in Section 11.4.3.

Thermal entrainment is not so important if the plume fluid is cold. Figure 11.5b shows a column of cold, dense, more viscous fluid descending into the same kind of fluid. The subdued head-and-tail structure is due to some of the surrounding fluid cooling and descending with the plume, but the resistance to the head from the surrounding lower-viscosity fluid is not sufficient to generate a significant internal circulation in the head, so there is no entrainment into it.

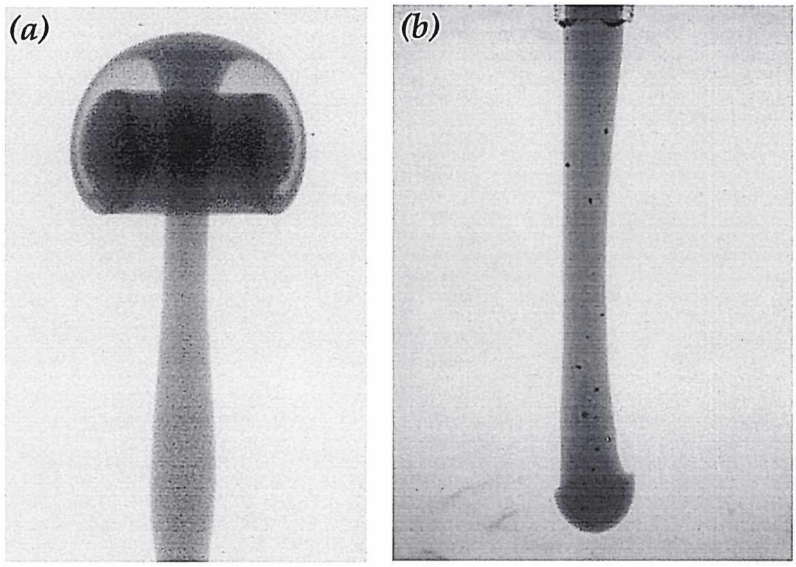

Figure 11.5. Thermal plumes in laboratory experiments, formed by injecting hot or cold dyed fluid into otherwise identical fluid. The fluid has a strong temperature dependence of viscosity. (a) The buoyant fluid is hot, and the plume viscosity is about 1/300 times that of the surrounding fluid. A spiral structure forms in the head due to thermal entrainment of ambient fluid. From Griffiths and Campbell [24]. (b) The injected fluid is cooler and hence denser and more viscous than the ambient fluid. There is little entrainment of cooled surrounding fluid, and only a very small head forms. From Campbell and Griffiths [25]. Copyright by Elsevier Science. Reprinted with permission.

Returning to the hot, low-viscosity plume of Figure 11.5a, similar structures are formed if a plume grows from a hot thermal boundary layer and the fluid viscosity is a strong function of temperature. Results of a numerical experiment scaled approximately to the mantle are shown in Figure 11.6. The panels are sections through an axisymmetric model showing the growth of a plume from an initial perturbation in the boundary layer. A line of passive tracers delineates the fluid initially within the hot boundary layer. The tracers reveal that the boundary layer fluid forms a spiral in the head due to thermal entrainment, as in Figure 11.5a. This numerical model also reveals the thermal structure within the plume. The hottest parts of the plume are the tail and the top of the head, where the tail material spreads out. Most of the head is cooler, and there are substantial thermal gradients within it. Temperatures within the head are intermediate between the plume tail temperature and the surrounding fluid.

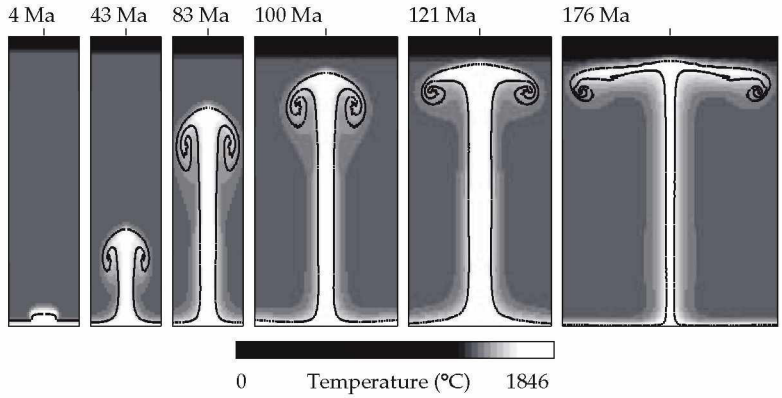

Figure 11.6. Sequence from a numerical model in which a plume grows from a thermal boundary layer. The model is axisymmetric and scaled approximately to the mantle. Viscosity is a strong function of temperature, and the ambient viscosity is 10^{22} Pa s. The bottom boundary temperature is 430 °C above the interior temperature, and the fluid viscosity there is about 1% of that of the interior fluid. A line of passive tracers delineates fluid initially within the thermal boundary layer.

11.4.2 Heads and tails

Here we look at why low-viscosity plumes form a head-and-tail structure. In the case in which the plume has a higher viscosity than the surroundings, the rise of the plume is limited mainly by the viscous resistance within the plume itself and within the boundary layer that feeds it. This means that the fluid in the plume does not rise faster than the top or head, and so it does not accumulate into a large head. The moderate variation of thickness with height is explained by the stretching of the column as the top rises faster than the stiff fluid can flow after it.

On the other hand, in the case where the plume has a lower viscosity, the plume fluid can flow readily from the boundary layer into and up the plume, and the main resistance to its rise comes from the surrounding more viscous fluid, which must be pushed out of the way. In this situation, the rise of the top of the plume is analogous to the rise of a buoyant sphere, and is regulated by the same balance of buoyancy and viscous resistance. In Chapter 6 we derived the Stokes formula for the velocity at which a buoyant sphere rises (Equation (6.8.3)). In fact you can see that the heads of the plumes in Figures 11.4b and 11.5a closely approximate a sphere. The role of this sphere is to force a path through the more viscous surroundings. Its rate of rise is initially slow, but it grows by the addition of plume fluid flowing out of the boundary layer. Once the head is large enough to force a path, the low-

viscosity plume fluid can readily follow, requiring only a narrow conduit to flow through, its rate of flow being regulated by the rate at which it can flow out of the thin boundary layer. This is why the conduit trailing the head can have a much smaller radius.

The way the head-and-tail structure of plumes depends on the viscosity contrast between the plume and its surroundings is illustrated further in Figure 11.7. This shows three numerical models of plumes with different ratios of plume viscosity to surrounding viscosity: respectively 1, 1/30 and 1/200. The size of the head is similar in each case, but the conduit is thinner for the lower viscosities, reflecting the fact that the lower viscosity material requires only a thin conduit for a similar rate of flow.

11.4.3 Thermal entrainment into plumes

We will now consider the thermal structure of plumes in more detail. As the hot fluid in the conduit reaches the top of the head, it spreads radially out and around the periphery of the sphere, becoming very thin because of the greater radius of the head (Figures 11.6, 11.7). Because it is thinned, its heat diffuses out much more quickly (remember, from Chapter 7, that a diffu-

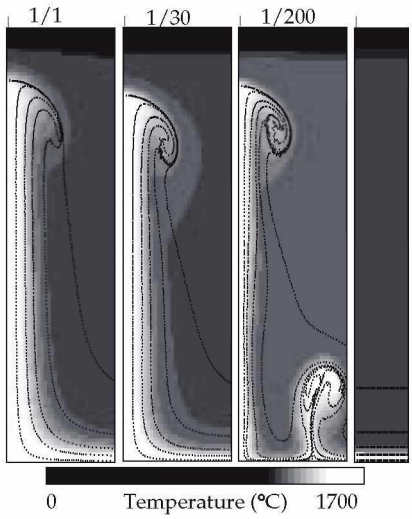

Figure 11.7. Plumes from three numerical models with different ratios of minimum plume viscosity to ambient viscosity, respectively 1, 1/30 and 1/200, showing how the tail is thinner for lower-viscosity plumes. The models are axisymmetric about the left-hand side of each panel. Several lines of tracers in this model mark fluid from different levels in the box. The initial configuration is shown in the right-hand panel. A secondary instability has developed in the right-hand model.

sion time scale is proportional to the square of the length scale involved). This heat goes partly outwards, to form the thermal boundary layer around the head, and partly inwards, to further heat the entrained material wrapping under it. As a result, the head has a temperature intermediate between that of the conduit and the surroundings. The spiral structure of the plume fluid, which is revealed by the dye in Figure 11.5a and by the tracers in Figures 11.6 and 11.7, is not evident in the thermal structure, because it is smoothed out by thermal diffusion. There are still thermal gradients in the head, but they are subdued relative to the temperature difference between the conduit and the surroundings.

The additional lines of tracers in Figure 11.7 reveal that most of the material entrained into the head comes from the lowest 10–20% of the fluid layer. Since these numerical experiments are scaled approximately to the mantle, this conclusion will apply also to plumes in the mantle. This is important for the interpretation of the geochemistry of flood basalts (Section 11.5).

We can quantify the rate of entrainment into a plume head using our understanding of thermal diffusion (Section 7.2) and of rising buoyant spheres (Section 6.8), following the approach used by Griffiths and Campbell [24]. The situation is sketched in Figure 11.8. We take the approach of using approximations that are rough, but that scale in the appropriate way. The thickness, δ, of the thermal boundary layer adjacent to the hot plume head will depend on the time the adjacent fluid is in contact with the passing plume head. This time will be of the order of $2R/U$, where the plume head radius is R and its rise velocity is U. Then, from Section 7.2,

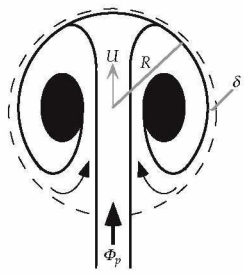

Figure 11.8. Sketch of a thermal boundary layer around a hot plume head. The fluid in the thermal boundary layer is heated by diffusion from the head. It is then buoyant and is entrained into the head. Boundary layer thickness is δ, head radius is R, head rise velocity is U and the volumetric flow rate up the plume tail is Φ_p.

$$\delta = \sqrt{\kappa t} = \sqrt{\frac{2\kappa R}{U}} \tag{11.4.1}$$

where κ is the thermal diffusivity. The horizontal cross-sectional area of the boundary layer near the head's equator is the head circumference times this thickness, $2\pi R\delta$, and the rate at which boundary layer fluid flows through this area is

$$\Phi_e = 2\pi R\delta U \tag{11.4.2}$$

We can assume that this fluid, or a constant fraction of it, becomes entrained into the head, so that Φ_e is an estimate of the volumetric rate of entrainment. The velocity, U, at which the head rises is given by the Stokes formula for a low-viscosity sphere (Section 6.8):

$$U = \frac{g\rho\alpha\Delta T R^2}{3\mu} \tag{11.4.3}$$

where ρ, α and μ are the density, thermal expansion coefficient and viscosity of the fluid respectively and ΔT is the temperature difference between the head and its surroundings.

If we take standard mantle values for these quantities (Appendix 2) with a viscosity appropriate for lower mantle, $\mu = 10^{22}$ Pa s, a temperature difference of 100 °C and a radius of 500 km, this yields a rise velocity of $U = 7 \times 10^{-10}$ m/s = 20 mm/a. The boundary layer thickness is then 40 km and the rate of entrainment is 2.7 km^3/a. This is comparable to the volume flow rate inferred for the Hawaiian plume tail of 7.5 km^3/a, which is the strongest plume tail by about a factor of 3 [11, 12]. The rate of increase of the head radius due to entrainment is

$$\frac{\partial R}{\partial t} = \frac{\Phi_e}{4\pi R^2} \tag{11.4.4}$$

With the values just derived, the rate of increase of radius is 1 mm/a = 1 km/Ma. This compares with a rise velocity of 20 mm/a.

This may suggest that entrainment is not very important, but Griffiths and Campbell integrated Equations (11.4.1–3), taking account of the influx from the tail, Φ_p, and the drop in average temperature as the entrainment proceeds. As cool fluid is entrained, the heat content of the plume is diffused through a larger volume. If the rate of inflow of fluid, Φ_p, is constant, the total heat supplied is proportional to $\Delta T_s \Phi_p (t - t_0) = \Delta T_s \Phi_p \Delta t$, where ΔT_s is the temperature excess of the source and Δt is the duration of the inflow. If the head volume at a later time is V, then conservation of energy requires that

$$\Delta T = \Delta T_s \Phi_p \Delta t / V \tag{11.4.5}$$

Combining Equations (11.4.1–3) with this yields

$$\Phi_e = 2\pi R \left[\frac{\kappa g \rho \alpha \Delta T_s \Phi_p \Delta t}{2\pi\mu} \right]^{1/2} \tag{11.4.6}$$

Then we can write an equation for the radius as a function of time as

$$\frac{\partial R}{\partial t} = \frac{\Phi_p + \Phi_e}{4\pi R^2} \tag{11.4.7}$$

Griffiths and Campbell found that plume head sizes of about 500 km radius at the top of the mantle are predicted rather consistently, independent of the tail flow rate and the temperature difference of the plume fluid source. Some of their results are shown in Figure 11.9. The initial rate of increase of the radius is much greater than it is as the head nears the top of the mantle, which explains the slow rates estimated above. Most of the curves in Figure 11.9 are for a mantle viscosity of 10^{22} Pa s, believed to be appropriate for the deep mantle where most of the head growth occurs. A lower viscosity of 10^{21} might be appropriate for the mantle in the Archean, and a smaller head is then predicted (Figure 11.9a). The plume head in the numerical experiment of Figure 11.6 approaches 1000 km in diameter near the top, consistent with their predictions. Taking the box depth to be 3000 km, the thermal halo in the fourth panel is 1000 km across and the tracers span about 800 km.

Entrainment may also occur into a plume tail. When the tail is vertical, as in Figures 11.6,7,10, this is so small that it is not evident in any obvious way. In fact Loper and Stacey have calculated that a strictly vertical plume tail with a strong viscosity contrast would entrain only a small percentage of additional material. Presumably this is because the travel time of the fluid up the conduit is short enough that diffusive heat loss to the surroundings is small. In the

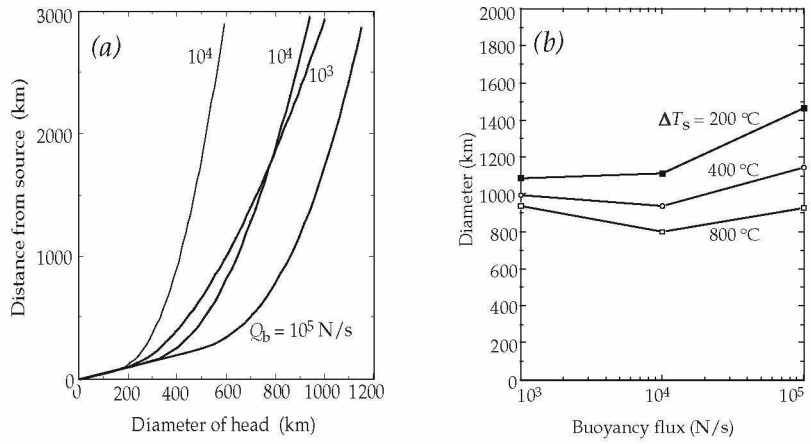

Figure 11.9. (a) Predicted plume head diameter versus height risen in a mantle of viscosity 10^{22} Pa s (heavy) and 10^{21} Pa s (light). Curves are labelled with buoyancy flow rate $Q_b = g\Delta\rho\Phi_p$. (b) Predicted plume head diameter at the top of the mantle for a mantle viscosity of 10^{22} Pa s and a range of buoyancy flow rates in the plume tail and fluid source excess temperatures, ΔT_s. From Griffiths and Campbell [24]. Copyright by Elsevier Science. Reprinted with permission.

numerical experiment depicted in the right-hand panel of Figure 11.7 the temperature in the centre of the conduit varies by only about 3% over most of its height. On the other hand, if the plume tail is inclined to the vertical, as it would be if the surrounding fluid were moving horizontally, then entrainment occurs by the same mechanism as for the plume head, and substantially larger degrees of entrainment may occur. This has been demonstrated experimentally by Richards and Griffiths [26].

11.4.4 Effects of a viscosity step and of phase changes

Figure 11.6 showed a numerical model of a thermal plume in which the viscosity depends on temperature. However, in the mantle the viscosity is also believed to vary substantially with depth, as discussed in Chapters 6 and 10. As well, phase transformations in the mantle transition zone may affect the rise of plumes, as discussed in Section 5.3, and the descent of subducted lithosphere discussed in Chapter 10.

The effects of including depth dependence of viscosity and a phase transformation are illustrated by the sequence from a numerical model shown in Figure 11.10. The viscosity increases with depth in a similar way to the models in Figure 10.12: there is a step by a factor of 20 at 700 km and an exponential increase by a factor of 10. As the plume head rises, its top feels the viscosity reducing and rises faster, stretching the plume head vertically.

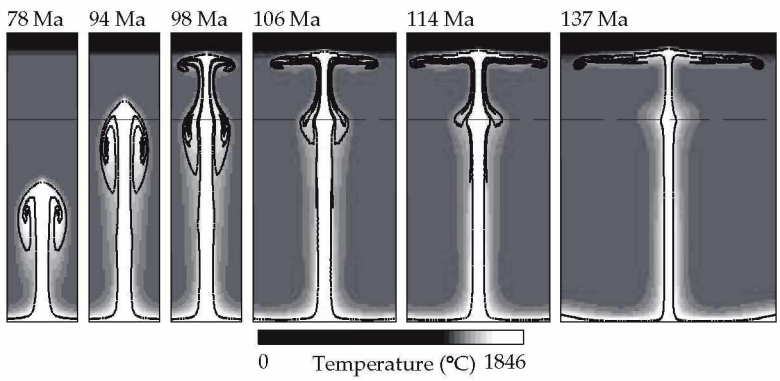

Figure 11.10. Sequence from a numerical plume model including increasing viscosity with depth and a phase transformation. The viscosity steps by a factor of 20 at 700 km depth and has an exponential increase by a factor of 10. The phase transformation at 700 km depth has a Clapeyron slope of −2 MPa/K. The plume slows and thickens through the phase transformation, but then narrows and speeds up in the low-viscosity upper layer.

This becomes pronounced as it enters the low-viscosity upper layer, where its rate of ascent increases and it necks down to a narrower diameter. As it then rises through the upper layer, it begins to form a second entrainment spiral, resulting in some convolution of the original spiral structure. The plume tail also speeds up and becomes narrower as it enters the upper layer (last frame).

This model also includes the effect of a phase transformation at 700 km depth with a moderately negative Clapeyron slope of −2 MPa/K. In this case the effect is not sufficient to block the ascent of the plume, though it does slow its rise in the vicinity of the phase transformation. This is most clearly evident in the last frame, where the plume tail bulges out as it slows, and then narrows again as it passes the phase transformation and enters the low-viscosity upper layer.

Compared with the plume in Figure 11.6, this plume reaches a shallower level. This is because it is much narrower as it rises into the upper mantle, and it does not trap as much mantle between itself and the lithosphere. Also as it spreads it is significantly thinner than in Figure 11.6, because of the lower viscosity below the lithosphere. Because it spreads faster, the high-temperature region is broader. These features are significant for the plume head model of flood basalts (Section 11.5), since they tend to promote greater melting over a broader area than in the model of Figure 11.6.

The effects of phase transformations with more negative Clapeyron slopes are illustrated by the models in Figure 11.11 [27]. As we have just seen in Figure 11.10, if the Clapeyron slope is −2 MPa/K, the plume continues through, and it is virtually unchanged except for a local bulge where its ascent is slowed by the phase transformation. If the Clapeyron slope is −3 MPa/K, then the plume is unable to penetrate. Apparently, if it does not penetrate immediately, then it spreads sufficiently rapidly that it

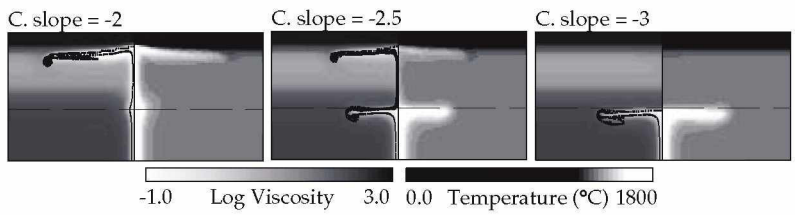

Figure 11.11. Plume models like that in Figure 11.10, but with different Clapeyron slopes (C. slope) of the phase transformation. The viscosity structure is shown on the left of these panels and the temperature on the right. From Davies [27]. Copyright by Elsevier Science. Reprinted with permission.

cannot ever penetrate. If the Clapeyron slope is −2.5 MPa/K, then the main part of the plume head penetrates but the tail is choked off and accumulates below the phase boundary. This would give rise to a tailless head in the upper mantle. (The precise value of the Clapeyron slope at which plume penetration is blocked is dependent on other details of the models, so these models should not be taken as a precise determination, but as a reasonable illustration of the process.)

11.5 Flood basalt eruptions and the plume head model

In Sections 11.1–3 we looked at observations that can be interpreted to relate to plume tails. It was the age-progressive volcanic chains that originally motivated Morgan's plume hypothesis, a model that we now identify more specifically as a plume tail. In 1981, Morgan [6] pointed out that several hotspot tracks emerged from flood basalt provinces. A notable example is the Chagos–Laccadive Ridge running south from the Deccan Traps flood basalt province in western India to Reunion Island in the Indian Ocean (Figures 4.3, 11.12).

Flood basalts are evidence of the largest volcanic eruptions identified in the geological record. They range up to 2000 km across, with accumulated thicknesses of basalt flows up to several kilometres. A map of the main identified flood basalt provinces is shown in Figure 11.12. Total volumes of extrusive eruptions range up to 10 million cubic kilometres, and evidence is accumulating that much of this volume is erupted in less than 1 million years [28]. It has been recognised within the past decade that some oceanic plateaus are oceanic equivalents of continental flood basalts. The largest flood basalt province is the Ontong–Java Plateau, a submarine plateau east of New Guinea.

Morgan [6] proposed that if flood basalts and hotspot tracks are associated, then the head-and-tail structure of a new plume, which had been demonstrated by Whitehead and Luther, would provide an explanation. Figure 11.13 illustrates the concept. The flood basalt eruption would be due to the arrival of the plume head, and the hotspot track would be formed by the tail following the head. If the overlying plate is moving, then the flood basalt and the underlying head remnant would be carried away, and the hotspot track would emerge from the flood basalt province and connect it to the currently active volcanic centre, which would be underlain by the active plume tail.

Not a lot of attention was given to Morgan's proposal until Richards, Duncan and Courtillot [23] revived and advocated the

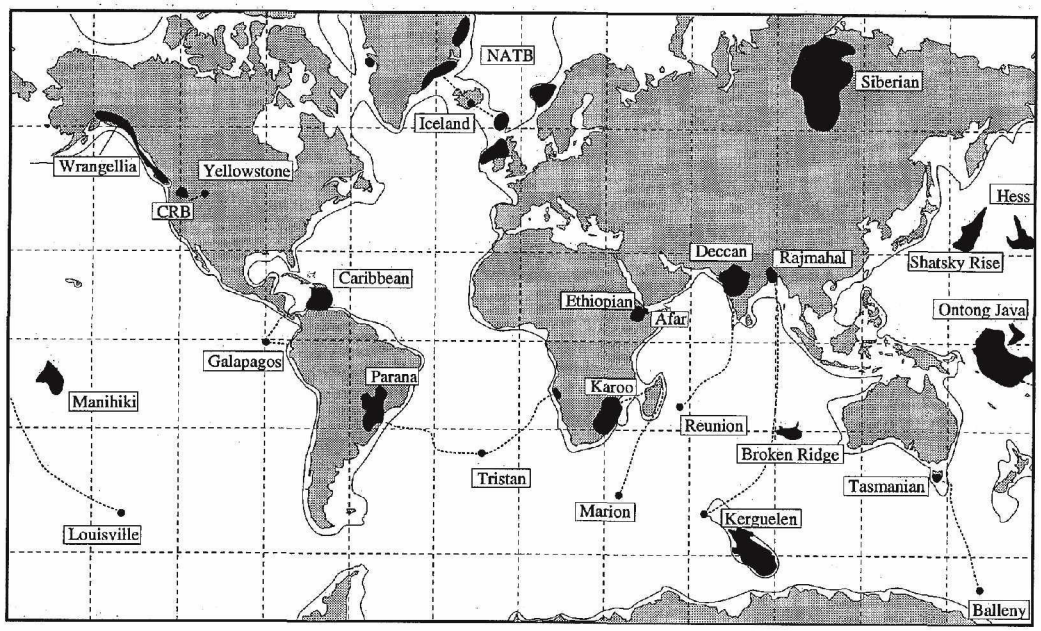

Figure 11.12. Map of continental and oceanic flood basalt provinces. Dotted lines show known or conjectured connections with active volcanic hotspots. After Duncan and Richards [2]. Copyright by the American Geophysical Union.

idea. Subsequently Griffiths and Campbell [17, 24] demonstrated the thermal entrainment process and argued in more detail for the plume head explanation of flood basalts. In particular Griffiths and Campbell argued that plume heads could reach much larger diametres, 800–1200 km, than had previously been estimated, if they rise from the bottom of the mantle, and also that they would

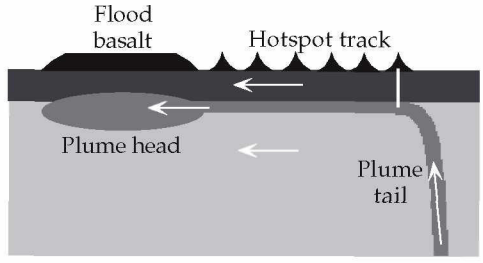

Figure 11.13. Sketch of the way a new plume with a head-and-tail structure can account for the relationship observed between some flood basalts and hotspot tracks, in which the hotspot track emerges from a flood basalt province and connects it to a currently active volcanic hotspot. It is assumed in the sketch that the plate and subjacent mantle are moving to the left relative to the plume source.

approximately double in horizontal diameter as they flattened and spread below the lithosphere (Figures 11.6, 11.10). This is in good agreement with the observed total extents of flood basalt provinces, the Karoo flood basalts being scattered over a region about 2500 km in diameter. Campbell and Griffiths argued that important aspects of the petrology and geochemistry of flood basalts could be explained by the model, in particular the concentration near the centres of provinces of picrites, which are products of higher degrees of melting than basalts. They argued that this can be explained by the temperature distribution of a plume head, which is hottest at the central conduit and cooler to the sides (Figure 11.6).

Though this model of flood basalt formation has attracted wide interest, it has not yet been fully explored quantitatively. The principal outstanding question is whether it can account quantitatively for the observed volumes of flood basalts in cases where there appears to have been little or no rifting. The perceived problem has been that normal mantle compositions do not begin to melt until they have risen to depths less than about 120 km even if they are 200 °C hotter than normal [29, 30]. Since continental lithosphere is commonly at least this thick, we would not expect plumes to melt at all under continents.

However plumes are known not to have normal mantle composition. It is widely recognised by geochemists on the basis of trace element contents that they have a larger complement of basaltic composition than normal mantle. This component of their composition is hypothesised to come from previously subducted oceanic crust that is entrained in plumes near the base of the mantle (Chapter 13; [21]). Such a composition would substantially lower the solidus temperature and enhance melt production. Some preliminary models [31] and continuing work indicate that melt volumes of the order of 1 million cubic kilometres can be produced from such a plume head. Examples of calculations of melt volume from a simplified plume head model with an enhanced basaltic component are shown in Figure 11.14. These show that it is plausible that several million cubic kilometres of magma could be erupted within about 1 Ma.

Other factors being evaluated for their influence on plume head melting are higher plume temperatures [32], the effect of mantle viscosity structure on the height to which plumes can penetrate, noted in Section 11.4.4 (Figure 11.10), or that plumes may be more effective at thinning the lithosphere and penetrating to shallow depths than has been recognised. The indications at this stage are that a satisfactory quantitative account of flood basalts will

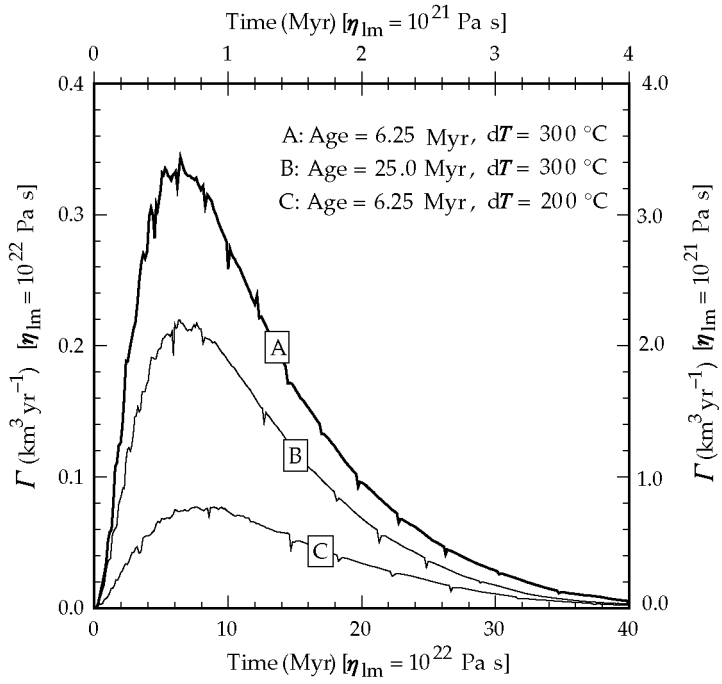

Figure 11.14. Calculated rates of magma generation, Γ, from a simplified numerical model of a plume head that includes 15% additional basaltic component. The curves assume different initial plume temperature excesses, dT, and different ages (and thus thicknesses) of lithosphere. The plume head was modelled as a sphere with initially uniform temperature. The left and bottom scales assume a mantle viscosity of 10^{22} Pa s, the right and top scales are for 10^{21} Pa s. From Cordery *et al.* [31]. Copyright by the American Geophysical Union.

emerge from the plume head model, but this has not yet been attained.

11.6 Some alternative theories

11.6.1 Rifting model of flood basalts

White and McKenzie [30] proposed a theory for the formation of very thick sequences of volcanic flows found along some continental margins and of flood basalt eruptions. The theory can usefully be separated into three parts. The first part is that the marginal volcanic provinces are produced when rifting occurs over a region of mantle that is hotter than normal because it is derived from a plume. This seems to give a very viable account of such provinces. The second part is that all flood basalts can be explained by this

mechanism. The third part is that the plume material is derived mainly from a plume tail, since they assumed that plumes are part of an upper mantle convection system and that plumes therefore derive from no deeper than 670 km. In this case the plume heads would have diameters of no more than about 300 km and volumes less than about 5% of a plume head from the bottom of the mantle [24].

The second part of White and McKenzie's model encounters the difficulty that a number of flood basalt provinces are said, on the basis of field evidence, to have erupted mainly before substantial rifting occurred (e.g. Deccan Traps) or in the absence of any substantial rifting (e.g. Siberian Traps, Columbia River Basalts) [33]. It also fails to explain the very short time scale of flood basalt eruptions, less than 1 Ma in the best-constrained cases. The third part of their model implies that a sufficient volume of warm mantle would take about 50 Ma to accumulate, but at the time the Deccan Traps erupted, India was moving north at about 180 mm/yr (180 km/Ma) so it would have traversed the extent of the flood basalts in only about 10 Ma. It is difficult to see how sufficient warm mantle could accumulate from a plume tail under such a fast-moving plate.

These difficulties are avoided by the plume head model of flood basalts, since the flow rate of the plume head is much greater than the tail and much of the melting is inferred to occur from beneath the intact lithosphere upon arrival of the plume head. It is true that the volumes of the eruptions have yet to be fully explained quantitatively, but current indications are that this is not a fundamental difficulty.

11.6.2 Mantle wetspots

Green [34] has argued that volcanic hotspots can be explained by mantle 'wetspots'. From a petrological point of view, this idea has some merits, since a small amount of water (less than 0.1%) can substantially reduce the solidus temperature, at which melting first occurs. It is also true that hydrated forms of minerals are generally less dense than their dry counterparts, which could provide the buoyancy required to explain hotspot swells. The effect on density needs to be better quantified, and it would need to be shown that observed water contents of hotspot volcanics are consistent with the amounts required to explain the buoyancy. It needs also to be shown that sufficient melt can be produced to explain the observed volcanism, since although water reduces the solidus temperature,

substantial degrees of melting still do not occur until the dry solidus temperature is approached.

However, a remaining difficulty would still be to explain the duration of long-lived volcanic centres like Hawaii. While a hydrated portion of the mantle, perhaps old subducted oceanic crust, might produce a burst of volcanism, there is no explanation offered for how the source might persist for 100 Ma or more. It is useful to estimate the volume of mantle required to supply the Hawaiian plume for 100 Ma. The total volume erupted into the Hawaiian and Emperor seamounts over 90 Ma is about $10^6\,\mathrm{km}^3$. If we assume that there was about 5% melting of the source, this requires a source volume of $2 \times 10^7\,\mathrm{km}^3$, equivalent to a sphere of diameter 340 km. If such a large and buoyant region existed as a unit in the mantle, it would rise and produce a burst of volcanism. To explain the Hawaiian volcanic chain the hydrated mantle material needs to be supplied at a small and steady rate.

The advantage of the thermal plume hypothesis is that a renewal mechanism is straightforwardly provided if the plume originates from a thermal boundary layer. It may be that the effects of water on melting and on plume buoyancy are significant, but it is far from clear that water alone could provide a sufficient explanation of the observations, while heat alone, or heat plus water, provides a straightforward and quantitatively successful account of the dynamical requirements of a theory of plumes.

11.6.3 Melt residue buoyancy under hotspot swells

J. P. Morgan and others [19] have proposed that the buoyancy supporting hotspot swells is due significantly also to the compositional buoyancy of the residue remaining after the hotspot magma has erupted. The residue will be less dense because iron partitions preferentially into the melt phase. However, the estimates made in Sections 11.2 and 11.3 indicate that the amount of melt produced is less than 1% of the volume of the plume material, in which case this will be a minor effect. Morgan and others estimate the density change of the residue as a function of mean melt fraction, f, from the formula

$$\Delta\rho = \rho_{\mathrm{m}}\beta f$$

where $\beta = 0.06$ is an empirically evaluated constant. This implies that the annual volume of mantle that arrives through the plume should expand by the same fraction, βf, and this expansion is what is manifest as the plume swell. We can therefore estimate the annual

contribution to the swell volume from the effect of residue buoyancy as

$$\Phi_{sr} = \Phi_p \beta f$$

Using the values $\Phi_p = 7.5\,km^3/a$ and $f = 0.01$, used earlier for Hawaii, this gives $\Phi_{sr} = 0.0045\,km^3/a$, which is only about 5% of the observed rate of swell formation of $0.1\,km^3/a$. While the residue buoyancy may be more significant locally under the volcanic chain, it seems that the direct buoyancy of the plume material is still required to account for most of the Hawaiian swell. This implies in turn that the estimates of buoyancy and heat flow rate given in Section 11.2 are reasonable.

11.7 Inevitability of mantle plumes

The earth is believed to have been strongly heated during the late stages of its formation. The heat comes from the release of gravitational energy of material falling onto the growing earth. The earth is believed to have formed from a disk of particles orbiting the sun and left over from the sun's formation. Models of the process of accumulation of material into larger bodies indicate that many bodies would grow simultaneously, but that there would be a wide distribution of sizes, with only a few large bodies and greater numbers of smaller bodies. In this situation the final stages of accumulation would involve the collision of very large bodies. A plausible and currently popular theory for the formation of the moon proposes that the moon was formed from the debris of a collision of a Mars-sized body with the earth. A collision of this magnitude would probably have melted much of the earth, and vaporised some of it. Accounts of these ideas can be found in [35, 36, 37].

Suppose that the earth was heated in this way, and that it quickly homogenised thermally, as a substantially liquid body would do. The temperature would not be uniform, but would follow an adiabatic profile with depth, due to the effect of pressure, as discussed in Chapter 7. The earth's temperature as a function of depth would therefore look like curve (a) sketched in Figure 11.15.

The earth would then lose heat through its surface. This would form an outer thermal boundary layer (a precursor to the lithosphere) and, with the mantle being very hot and possibly partially molten, rapid mantle convection could be expected. In this way the mantle would be cooled. Suppose, for the simplicity of this argument, that the entire mantle convected and cooled in this way.

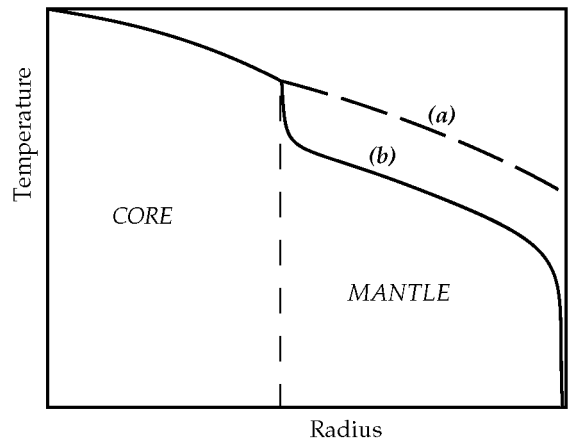

Figure 11.15. Sketch of the form of the temperature profile within the earth (a) soon after formation, and (b) later, after the mantle has cooled by heat loss to the surface. The core can only begin to lose heat after the mantle has become cooler than the core. Thereafter the heat conducting from the core into the base of the mantle forms a thermal boundary layer that can generate buoyant upwellings.

After some time, the temperature profile would have looked like curve (b) of Figure 11.15.

Initially, the core would not have been able to lose heat, because we assumed that the mantle and core had the same temperature at their interface. However, as the mantle cooled, heat would begin to conduct out of the core into the base of the mantle, and cooling of the core would commence. This heat from the core would form a thermal boundary layer at the base of the mantle, depicted in curve (b) of Figure 11.15. If the mantle viscosity were sufficiently low and the heat flow from the core sufficiently high, both of which are highly likely, this thermal boundary layer would become unstable and buoyant upwellings would rise from it. These upwellings would have a lower viscosity than the mantle they were rising through, so they would develop a head-and-tail structure, as discussed in Section 11.4.

Thus we have a general argument for the existence of thermal plumes in the mantle. The assumptions are that the core and mantle started with similar temperatures at their interface, that the mantle has been cooling, and that the conditions are such that the relevant Rayleigh number is greater than its critical value for instability and convection to occur. If the earth, now or in the past, functioned as more than two independent layers, then the argument generalises very simply: the layers would cool from the outside inwards, and

plumes would be generated in each layer by heat conducting from the next deeper layer.

11.8 The plume mode of mantle convection

We have seen that the existence of volcanic island and seamount chains terminating in isolated active volcanic hotspots, such as Hawaii, and surrounded by broad topographic swells imply the existence of narrow, long-lived columns of buoyant, rising mantle material. Morgan called these mantle plumes. The buoyancy and excess melting can be explained if the plumes are 200–300 °C hotter than normal mantle, and their longevity is plausible if they derive from a hot thermal boundary layer. Their higher temperature implies that plumes would have lower viscosity than normal mantle. Fluid dynamics experiments show that the preferred form of low-viscosity buoyant upwellings is columnar, and that new plumes would start with a large, spherical head. Plume heads are calculated to reach diameters of about 1000 km near the top of the mantle, and they provide a plausible explanation for flood basalt eruptions. The association of plume heads with their following plume tails provides an explanation for hotspot tracks that emerge from flood basalt provinces.

Plumes and the flow they drive in surrounding mantle comprise a distinct mode of mantle convection, driven by a hot, lower thermal boundary layer. They therefore complement the plate mode driven by the cool, top thermal boundary layer. As with the plate mode, there will be a passive downward return flow driven by plumes that balances the upflow in plumes. The fact that hotspot locations do not correlate strongly with the current configuration of plates (Figure 11.1; [38]) indicates that the plume and plate modes are not strongly coupled. The implication is that plumes rise through the plate-scale flow without substantially disrupting it. Experiments have shown that plume tails can rise through a horizontal background flow, bending away from the vertical but retaining their narrow tubular form [39, 40, 41]. However, there is a correlation between plume locations, broad geoid highs and slower seismic wavespeeds in the deep mantle [38, 42], indicating that plumes form preferentially away from deeply subducted lithosphere.

Plumes may have been significant tectonic agents through much of earth history. They may trigger ridge jumps or occasional larger-scale rifting events [5, 43]. Plume heads have been proposed as the direct source of Archean greenstone belts and the indirect cause, through their heat, of associated granitic terrains from sec-

ondary crustal melting [44]. They may have been a significant source of continental crust, directly from continental flood basalts and through the accretion as exotic terrains of oceanic flood basalts [14, 45]. They may be the source of many dike swarms, and as a source of heat they may have been involved in some regional 'anorogenic' crustal heating and melting events and in the reworking and mineralising of a significant proportion of the continental crust [14]. The term 'plume tectonics' has been used to encapsulate their possibly substantial tectonic role [14].

A fundamental aspect of mantle convection is that the thermal boundary layers are distinct agents, as I stressed in Chapter 8. It is therefore incorrect to regard plumes and plume tectonics as a possible substitute for plate tectonics, as has been speculated not infrequently for the early earth and for Venus. Currently in the earth, plate tectonics cools the mantle. If plate tectonics did not operate, then the top boundary layer would have to operate in another way in order to remove heat from the mantle. The role of plumes is to transfer heat from the layer below (the core) into the convecting mantle. Any surface heat flow or tectonic effect from plumes is incidental, and adds to whatever tectonics are driven by the top boundary layer. This will be discussed in more detail in Chapter 14.

A further implication of this last point is that the level of activity of plumes depends on the strength of the hot thermal boundary layer at the base of the mantle. This may have varied with time, though calculations suggest that it may have been rather constant (Chapter 14). It follows also that the two thermal boundary layers need to be prescribed separately in numerical models of mantle convection. In other words, it is sensible to define separate Rayleigh numbers for each thermal boundary layer, and hence for each mode of mantle convection.

11.9 References

1. T. S. Crough and D. M. Jurdy, Subducted lithosphere, hotspots and the geoid, *Earth Planet. Sci. Lett.* **48**, 15–22, 1980.
2. R. A. Duncan and M. A. Richards, Hotspots, mantle plumes, flood basalts, and true polar wander, *Rev. Geophys.* **29**, 31–50, 1991.
3. J. T. Wilson, A possible origin of the Hawaiian islands, *Can. J. Phys.* **41**, 863–70, 1963.
4. W. J. Morgan, Convection plumes in the lower mantle, *Nature* **230**, 42–3, 1971.
5. W. J. Morgan, Plate motions and deep mantle convection, *Mem. Geol. Soc. Am.* **132**, 7–22, 1972.

6. W. J. Morgan, Hotspot tracks and the opening of the Atlantic and Indian Oceans, in: *The Sea*, C. Emiliani, ed., Wiley, New York, 443–87, 1981.
7. K. C. Burke and J. T. Wilson, Hot spots on the earth's surface, *Sci. Am.* **235**, 46–57, 1976.
8. M. A. Richards, B. H. Hager and N. H. Sleep, Dynamically supported geoid highs over hotspots: observation and theory, *J. Geophys. Res.* **93**, 7690–708, 1988.
9. A. B. Watts and U. S. ten Brink, Crustal structure, flexure and subsidence history of the Hawaiian Islands, *J. Geophys. Res.* **94**, 10 473–500, 1989.
10. D. L. Turcotte and G. Schubert, *Geodynamics: Applications of Continuum Physics to Geological Problems*, 450 pp., Wiley, New York, 1982.
11. G. F. Davies, Ocean bathymetry and mantle convection, 1. Large-scale flow and hotspots, *J. Geophys. Res.* **93**, 10 467–80, 1988.
12. N. H. Sleep, Hotspots and mantle plumes: Some phenomenology, *J. Geophys. Res.* **95**, 6715–36, 1990.
13. F. D. Stacey, *Physics of the Earth*, 513 pp., Brookfield Press, Brisbane, 1992.
14. R. I. Hill, I. H. Campbell, G. F. Davies and R. W. Griffiths, Mantle plumes and continental tectonics, *Science* **256**, 186–93, 1992.
15. F. D. Stacey and D. E. Loper, Thermal histories of the core and mantle, *Phys. Earth Planet. Inter.* **36,** 99–115, 1984.
16. R. P. Von Herzen, M. J. Cordery, R. S. Detrick and C. Fang, Heat flow and thermal origin of hotspot swells: the Hawaiian swell revisited, *J. Geophys. Res.* **94**, 13 783–99, 1989.
17. I. H. Campbell and R. W. Griffiths, Implications of mantle plume structure for the evolution of flood basalts, *Earth Planet. Sci. Lett.* **99**, 79–83, 1990.
18. D. A. Clague and G. B. Dalrymple, Tectonics, geochronology and origin of the Hawaiian-Emperor volcanic chain, in: *The Eastern Pacific Ocean and Hawaii*, E. L. Winterer, D. M. Hussong and R. W. Decker, eds., Geological Society of America, Boulder, CO, 188–217, 1989.
19. J. P. Morgan, W. J. Morgan and E. Price, Hotspot melting generates both hotspot swell volcanism and a hotspot swell?, *J. Geophys. Res.* **100**, 8045–62, 1995.
20. P. Wessel, A re-examination of the flexural deformation beneath the Hawaiian islands, *J. Geophys. Res.* **98**, 12 177–90, 1993.
21. A. W. Hofmann and W. M. White, Mantle plumes from ancient oceanic crust, *Earth Planet. Sci. Lett.* **57**, 421–36, 1982.
22. J. A. Whitehead and D. S. Luther, Dynamics of laboratory diapir and plume models, *J. Geophys. Res.* **80**, 705–17, 1975.
23. M. A. Richards, R. A. Duncan and V. E. Courtillot, Flood basalts and hot-spot tracks: plume heads and tails, *Science* **246**, 103–7, 1989.

24. R. W. Griffiths and I. H. Campbell, Stirring and structure in mantle plumes, *Earth Planet. Sci. Lett.* **99**, 66–78, 1990.
25. I. H. Campbell and R. W. Griffiths, The evolution of the mantle's chemical structure, *Lithos* **30**, 389–99, 1993.
26. M. A. Richards and R. W. Griffiths, Deflection of plumes by mantle shear flow: experimental results and a simple theory, *Geophys. J.* **94**, 367–76, 1988.
27. G. F. Davies, Penetration of plates and plumes through the mantle transition zone, *Earth Planet. Sci. Lett.* **133**, 507–16, 1995.
28. M. F. Coffin and O. Eldholm, Large igneous provinces: crustal structure, dimensions and external consequences, *Rev. Geophys.* **32**, 1–36, 1994.
29. D. P. McKenzie and M. J. Bickle, The volume and composition of melt generated by extension of the lithosphere, *J. Petrol.* **29**, 625–79, 1988.
30. R. White and D. McKenzie, Magmatism at rift zones: the generation of volcanic continental margins and flood basalts, *J. Geophys. Res.* **94**, 7685–730, 1989.
31. M. J. Cordery, G. F. Davies and I. H. Campbell, Genesis of flood basalts from eclogite-bearing mantle plumes, *J. Geophys. Res.* **102**, 20 179–97, 1997.
32. C. Farnetani and M. A. Richards, Numerical investigations of the mantle plume initiation model for flood basalt events., *J. Geophys. Res.* **99**, 13 813–33, 1994.
33. P. R. Hooper, The timing of crustal extension and the eruption of continental flood basalts, *Nature* **345**, 246–9, 1990.
34. D. H. Green and T. J. Falloon, Pyrolite: A Ringwood concept and its current expression, in: *The Earth's Mantle: Composition, Structure and Evolution*, I. N. S. Jackson, ed., Cambridge University Press, Cambridge, 311–78, 1998.
35. G. W. Wetherill, Occurrence of giant impacts during the growth of the terrestrial planets, *Science* **228**, 877–9, 1985.
36. G. W. Wetherill, Formation of the terrestrial planets, *Annu. Rev. Astron. Astrophys.* **18**, 77–113, 1980.
37. H. E. Newsom and J. H. Jones, *Origin of the Earth*, 378, Oxford University Press, New York, 1990.
38. M. Stefanick and D. M. Jurdy, The distribution of hot spots, *J. Geophys. Res.* **89**, 9919–25, 1984.
39. M. A. Richards and R. W. Griffiths, Thermal entrainment by deflected mantle plumes, *Nature* **342**, 900–2, 1989.
40. R. W. Griffiths and I. H. Campbell, On the dynamics of long-lived plume conduits in the convecting mantle, *Earth Planet. Sci. Lett.* **103**, 214–27, 1991.
41. R. W. Griffiths and M. A. Richards, The adjustment of mantle plumes to changes in plate motion, *Geophys. Res. Lett.* **16**, 437–40, 1989.
42. M. A. Richards and D. C. Engebretson, Large-scale mantle convection and the history of subduction, *Nature* **355**, 437–40, 1992.

43. R. I. Hill, Starting plumes and continental breakup, *Earth Planet. Sci. Lett.* **104**, 398–416, 1991.
44. I. H. Campbell and R. I. Hill, A two-stage model for the formation of the granite-greenstone terrains of the Kalgoorlie-Norseman area, Western Australia, *Earth Planet. Sci. Lett.* **90**, 11–25, 1988.
45. M. A. Richards, D. L. Jones, R. A. Duncan and D. J. DePaolo, A mantle plume initiation model for the Wrangellia flood basalt and other oceanic plateaus, *Science* **254**, 263–7, 1991.

CHAPTER 8

Convection

Convection is a kind of fluid flow driven by internal buoyancy. In general, the buoyancy that drives convection derives from horizontal density gradients. In the mantle, the main sources of density gradients are horizontal thermal boundary layers. Convection is driven when the buoyancy (positive or negative) of a thermal boundary layer causes it to become unstable, so that fluid from it leaves the boundary of the fluid and rises or falls through the interior of the fluid. This statement may seem to be labouring the obvious, but there has been a lot of confusion about the nature of mantle convection, and much of this confusion can be avoided by keeping these basic ideas clearly in mind.

In general the buoyancy driving convection may be of thermal or compositional origin. We will be concerned mainly with thermal buoyancy, but compositional buoyancy is also important in the mantle. It is best to consider first thermal convection, that is convection driven by thermal buoyancy. Some aspects of compositional buoyancy will be considered in Chapter 14.

Here I describe sources of buoyancy, give a simple example of thermal convection, and show how there is an intimate relationship between convection and the surface topography that it produces. This establishes some basic concepts that will be applied more explicitly to the mantle in subsequent chapters.

In the course of doing this, I show how convection problems scale, how the Rayleigh number encapsulates this scaling, why convection occurs only if the fluid is heated or cooled strongly enough, and how the mode of heating (from below or internally) governs the nature of the thermal boundary layers. In principle there may be two thermal boundary layers in a fluid layer, one at the top and one at the bottom, or there may be only one, depending on the way the fluid is heated and cooled.

8.1 Buoyancy

Buoyancy arises from gravity acting on density differences. Technically, buoyancy is used to describe a *force*. Thus it is not the same as a density difference. Rather, it is the product of a density difference, $\Delta\rho$, a volume, V, and the gravitational acceleration, g:

$$B = -gV\Delta\rho = -g\Delta m \tag{8.1.1}$$

where Δm is the mass anomaly due to a volume V with a density difference $\Delta\rho = \rho_V - \rho$ from its surroundings. The minus is used because, in common usage, buoyancy is positive upwards, whereas gravity and weight are positive downwards. Thus for a density excess, $\Delta\rho$ is positive and B is negative, that is downwards.

It is buoyancy rather than just density difference that is important in convection. A large density difference within a small volume may be unimportant. For example, you might expect intuitively that a steel ball-bearing, 1 cm in diameter, embedded in the mantle would not sink rapidly to the core, despite a density difference of over 100%. On the other hand, a plume head with a density contrast of only about 1% would have a significant velocity if its diameter were 1000 km, as we saw in Section 6.8.

With thermal buoyancy, density differences arise from thermal expansion. This is described by

$$\rho = \rho_0[1 - \alpha(T - T_0)] \tag{8.1.2}$$

where ρ is density, α is the volume coefficient of thermal expansion, T is temperature, and ρ_0 is the density at a reference temperature T_0. With α typically about $3 \times 10^{-5}/^{\circ}\mathrm{C}$ (Table 7.3), a temperature contrast of 1000 °C gives rise to a density contrast of about 3%. In the lower mantle, where α may be only about $1 \times 10^{-5}/^{\circ}\mathrm{C}$ due to the effect of pressure, the corresponding density difference would be only about 1%.

There are some density differences in the earth larger than these thermal density differences, and these are due to differences in chemical or mineralogical composition. For example the oceanic crust has a density of about $2.9\,\mathrm{Mg/m^3}$, compared with an upper mantle density of about $3.3\,\mathrm{Mg/m^3}$, so it has a density deficit of about $400\,\mathrm{kg/m^3}$ or 12%. The total density change through the mantle transition zone is about 15%. Much or all of this is believed to be due to pressure-induced phase transformations of the mineral assemblage (Chapter 5), and so it is not necessarily a source of buoyancy. However, locally all of the density differences associated

with particular transformations may be operative because the depth of the transformation is changed by temperature, as was discussed in Chapter 5. Apart from this, if the density increase through the transition zone is not all due to phase transformations, the maximum that could be attributed to a difference between the composition of the upper mantle and the lower mantle is a small percentage, according to the seismological and material property constraints discussed in Chapter 5.

It is useful to have some idea of the magnitudes of buoyancies of various objects. For example, a ball bearing would exert a buoyancy force of about $-0.02\,\mathrm{N}$ (taking buoyancy to be positive upwards), while a plume head 1000 km in diameter with a temperature difference of 300 °C would have a buoyancy of about $2 \times 10^{20}\,\mathrm{N}$. Subducted lithosphere extending to a depth of 600 km exerts a buoyancy of about $-40\,\mathrm{TN}$ per metre of oceanic trench, that is per metre horizontally in the direction of strike of the subducted slab.

If the subducted lithosphere extended to the bottom of the mantle, about 3000 km in depth, its buoyancy would be about $-200\,\mathrm{TN/m}$. Comparing this with a plume head, it takes a piece of subducted lithosphere about 1000 km wide and 3000 km deep to equal in magnitude the buoyancy of a plume head. While this may make plume heads seem to be very important, you should bear in mind that the total length of oceanic trenches is over 30 000 km. Thus, while the buoyancy of a plume head is impressive, it is still small compared to the total buoyancy of subducted lithosphere.

The crustal component of subducted lithosphere undergoes a different sequence of pressure-induced phase transformations than the mantle component, and as a result it is sometimes less dense and sometimes denser than the surrounding mantle, with the difference usually no more than about $200\,\mathrm{kg/m^3}$ (Section 5.3.4). Even if it had the same density difference, say $-100\,\mathrm{kg/m^3}$, extending throughout the mantle, its thickness is only about 7 km and its total contribution to slab buoyancy would be only about 20 TN/m, compared with the slab thermal buoyancy of $-200\,\mathrm{TN/m}$. This suggests that normally the crustal component of subducted lithosphere does not substantially affect the slab buoyancy. However, if the subducted lithosphere is young, so that its negative thermal buoyancy is small, the crustal buoyancy may be more important. This may have been more commonly true at earlier times in earth history. These possibilities will be taken up again in Chapter 14.

The very large range of the magnitudes of buoyancies of the various objects just considered serves to emphasise that we must

consider the volume occupied by anomalous density, not just the magnitude of the density anomaly itself.

8.2 A simple quantitative convection model

We are now ready to consider a convection model that is simple in concept but goes to the heart of plate tectonics and its relationship with mantle convection. The approach was first used by Turcotte and Oxburgh in 1967 [1]. At that time plate tectonics was only just beginning to gain acceptance amongst geophysicists. I give a simplified version here. A more detailed version is given by Turcotte and Schubert [2], p. 279. I also acknowledge that it is only within the last five years or so that numerical models have become substantially superior to Turcotte and Oxburgh's approximate analytical model. Such is the power of capturing the simple essence of a problem.

Consider plates on a viscous mantle, as sketched in Figure 8.1a. The plates comprise a thermal boundary layer, within which the temperature changes from the surface temperature to the temperature within the interior of the mantle. Because the plates are cold, they are denser and prone to sink: they have negative buoyancy. In Figure 8.1a, one plate is depicted as subducting, and we presume here that it is sinking under its own weight. As the subducted part sinks, it drags along the surrounding viscous mantle with it. The motion of the plate is resisted by the viscous stresses accompanying

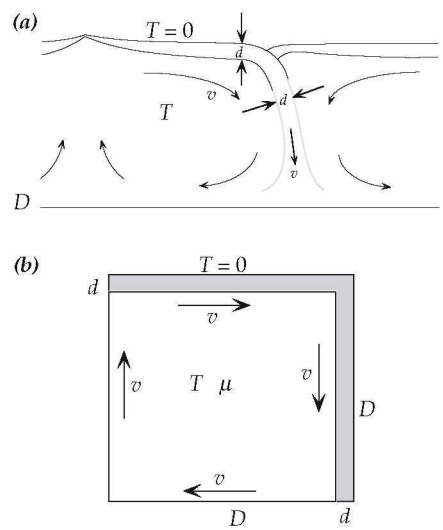

Figure 8.1. (a) Sketch of flow driven by a subducting plate. (b) Idealised form of the situation in (a).

this mantle flow. The viscous stresses are proportional to velocity. This permits an equilibrium to develop between the opposing forces: the velocity adjusts until the resistance balances the buoyancy.

Our approach is based on the same principle as that used in Chapter 6 when we considered flow down a pipe that is driven by the fluid's own weight, and the rise of a buoyant sphere. In each case, there was a balance between a buoyancy force and a viscous resistance. The system achieves balance by adjusting its velocity until the viscous resistance balances the buoyancy. This balance is stable, in the sense that a change in the velocity will induce an imbalance of the forces that will quickly return the velocity to its equilibrium value. However, we should remember that the motions are so slow in the mantle that accelerations and momenta are quite negligible, and the forces are essentially in balance at every instant, though their magnitudes may slowly change in concert.

Let us make a simple dimensional estimate of the balance between buoyancy and viscous forces, in the same way as we did for the buoyant sphere in Chapter 6. Here, because the two-dimensional sketch is assumed to be a cross-section through a structure that extends in the third dimension, the forces will be calculated per unit length in the third dimension. Let us also simplify the geometry into that depicted in Figure 8.1b.

First consider the buoyancy of the lithosphere descending down the right side of the box. Assume that this lithosphere simply turned and descended, preserving its thickness and temperature profile. From the basic formulas (8.1.1) and (8.1.2), the buoyancy is

$$B = g \cdot Dd \cdot \rho\alpha\Delta T$$

where ΔT is the average difference in temperature between the descending lithosphere and the fluid interior. This is approximately $\Delta T = -T/2$, where T is the temperature of the interior fluid. (We used the same approximation in estimating the subsidence of oceanic lithosphere in Section 7.4). Thus

$$B = -g \cdot Dd\rho\alpha T/2 \tag{8.2.1}$$

If we want to evaluate this expression, we can independently estimate the values of all quantities except the thickness, d, of the lithosphere upon subduction. This is just the thickness of the layer that has cooled by conduction of heat to the surface, as we considered in Section 7.3. It is determined by the amount of time the subducting piece of lithosphere spent at the surface. This time is

$t = D/v$. According to the discussion of thermal diffusion in Chapter 7, the thickness of the layer from which heat has diffused is approximated by

$$d = \sqrt{\kappa t} = \sqrt{\kappa D/v} \tag{8.2.2}$$

where κ is the thermal diffusivity. So we have an expression for d, but now it includes the still-unknown quantity v. We will see below how to deal with it.

Now consider the viscous resistance. As with our rough estimate for a buoyant sphere (Section 6.8.1), we estimate the viscous stresses from a characteristic velocity gradient. In this case, the velocity changes from v to $-v$ across the dimensions of the box, so a representative velocity gradient is $2v/D$. The resisting viscous stress σ acting on the side of the descending slab is then

$$\sigma = \mu \cdot 2v/D$$

This is a force per unit area. We get the force per unit length (in the third dimension) by multiplying σ by the vertical length, D, of the slab:

$$R = D\sigma = D \cdot 2\mu v/D = 2\mu v \tag{8.2.3}$$

The buoyancy and resistance are balanced when $B + R = 0$. From (8.2.1) and (8.2.3), this occurs when

$$v = -g \cdot Dd\rho\alpha T/4\mu \tag{8.2.4}$$

This expression for v also involves d. We can combine Equations (8.2.2) and (8.2.4) to solve for the two unknowns v and d. The result is

$$v = D\left(\frac{g\rho\alpha T\sqrt{\kappa}}{4\mu}\right)^{2/3} \tag{8.2.5}$$

Using $D = 3000\,\text{km}$, $\rho = 4000\ \text{kg/m}^3$, $\alpha = 2 \times 10^{-5}/^\circ\text{C}$, $T = 1400\,^\circ\text{C}$, $\kappa = 10^{-6}\,\text{m}^2/\text{s}$ and $\mu = 10^{22}\,\text{Pa s}$, this yields $v = 2.8 \times 10^{-9}\,\text{m/s} = 90\,\text{mm/a}$. This is quite a good estimate of the velocity of the faster plates.

Other quantities can be estimated from these results. From Equation (8.2.2), the thickness of the lithosphere is 33 km. This is of the same order of magnitude as the observed oceanic lithosphere, though about a factor of two too small. If we had used the more accurate estimate of $d = 2\sqrt{(kt)}$ that is obtained from the

error function solution for the cooling lithosphere (Equation (7.3.3)), we would have obtained 66 km. Also our estimate of the time the lithosphere spent cooling at the surface is a bit small, because we assumed implicitly in Figure 8.1b that the plate is only as wide as the mantle is deep, that is about 3000 km. At a velocity of 90 mm/a = 90 km/Ma, the plate will be only 33 Ma old when it subducts. Observed lithosphere of this age is about 60 km thick. If the box were longer, the plate would be older and thicker. This problem is left as an Exercise.

The surface heat flux, q, can also be estimated from the temperature gradient through the boundary layer: $q = KT/d$, where K is the thermal conductivity. Using $K = 3\,\mathrm{W/m\,K}$, this gives $q = 130\,\mathrm{mW/m^2}$. This compares with an observed heat flux of about $90\,\mathrm{mW/m^2}$ for lithosphere of this age, and a mean heat flux of about $100\,\mathrm{mW/m^2}$ for the whole sea floor.

The point of these estimates is not that they are not very accurate, but that they are of the right order of magnitude. In the absence of the simple theory developed above, one could not make a sensible estimate even of the orders of magnitude to be expected. Given the crudity of the approximations made, the agreement within about a factor of two is very good, perhaps better than is really justified.

The agreement of these estimates with observations suggests that we have a viable theory for mantle convection that explains why plates move at their observed velocities. Think about the significance of that statement for a moment. Plate tectonics is recognised as a fundamental mechanism driving geological processes. Within a few pages, with some simple physics and simple approximations, we have produced a theory that is consistent with some primary observations of plate tectonics (their velocities, thicknesses and heat fluxes). We thus have a candidate theory for the underlying mechanism for a very wide range of geological processes. We will be further testing the viability (and sufficiency) of this theory through much of the rest of this book.

8.3 Scaling and the Rayleigh number

The approximate theory just developed yields not only reasonable numerical estimates of observed quantities, but also information on how these quantities should scale. Thus, for example, according to Equation (8.2.5), if the viscosity were a factor of 10 lower at some earlier time in earth history, the plate velocities would not be 10 times greater, but $10^{2/3} = 4.6$ times greater. Similarly, we can combine Equations (8.2.2) and (8.2.5) and deduce that

$$\left(\frac{D}{d}\right)^3 = \frac{g\rho\alpha T D^3}{4\kappa\mu} \tag{8.3.1}$$

This implies that the boundary layer thickness would have been 2.15 times less (15 km) and the heat flow 2.15 times higher (275 mW/m^2) with a viscosity 10 times lower.

Equation (8.3.1) is written in this particular form to make a more general point. The left side involves a ratio of lengths, and it is therefore dimensionless. One can work through the dimensions of the right side and confirm that it is also dimensionless, as it should be. This particular, rather arbitrary looking, collection of constants actually encapsulates the scaling properties that we have just looked at, and others besides. In fact it encapsulates many of the scaling properties of convection in a fluid layer in general, not just the mantle convection we are concerned with here. For this reason it has been recognised by fluid dynamicists as having a fundamental significance for all forms of thermal convection. It was Lord Rayleigh who first demonstrated this, and this dimensionless combination (without the numerical factor) is known as the Rayleigh number in his honour. It is usually written

$$Ra = \frac{g\rho\alpha T D^3}{\kappa\mu} \tag{8.3.2}$$

For the mantle, using values used in the last section, we can estimate that $Ra \approx 3 \times 10^6$.

We can see explicitly the way in which the Rayleigh number encapsulates the scaling properties by rewriting the above results in terms of Ra. Thus, from Equation (8.3.1),

$$d/D \sim Ra^{-1/3} \tag{8.3.3}$$

where '$\sim$' implies proportionality and 'of the order of'. The ratio d/D is obviously dimensionless also, and we can view this ratio as a way of scaling d, relative to a length scale that is characteristic of the problem, namely the depth of the fluid layer, D. Similarly, from Equation (8.2.5)

$$v(D/\kappa) \equiv v/V \sim Ra^{2/3} \tag{8.3.4}$$

The dimensions of κ are (length^2/time), so the ratio κ/D has the dimensions of velocity. We can thus regard $V = \kappa/D$ as a velocity scale characteristic of the problem. Then Equation (8.3.4) shows how the actual flow velocity v relates to the velocity scale V derived

from the geometry of the problem and the properties of the material.

Fluid dynamicists are enamoured of these dimensionless ratios, for the very good reason that they encapsulate important scaling information, and they have named lots of them after people. Thus the combination vD/κ is called the Peclet number, written Pe:

$$Pe \equiv vD/\kappa = v/V \tag{8.3.5}$$

Then Equation (8.2.5) reduces to $Pe \sim Ra^{2/3}$. Using values from the last section, we can estimate that for the mantle $Pe \approx 9000$.

I will not go through an exhaustive catalogue of these dimensionless numbers here, but a couple of further examples are worth noting. First, it is instructive to combine the scaling quantities V and D to define a characteristic time:

$$t_\kappa \equiv D/V = D^2/\kappa \tag{8.3.6}$$

From Chapter 7, this can be recognised as a diffusion time scale. It is an estimate of the time it would take the fluid layer to cool significantly by thermal diffusion, that is by conduction, in the absence of convection. Compare this with a time scale that is more characteristic of the convection process: $t_v = D/v$. This is the time it takes the fluid to traverse the depth of the fluid layer at the typical convective velocity, v, so it can be called the transit time. From Equations (8.3.4) and (8.3.6),

$$t_v = D/v = t_\kappa Ra^{-2/3} \tag{8.3.7}$$

If $Ra = 3 \times 10^6$, then $t_v = 5 \times 10^{-5} t_\kappa$. Thus if Ra is large, t_v is much smaller than t_κ, reflecting the fact that, at high Rayleigh numbers, convection is a much more efficient heat transport mechanism than conduction.

Actually Equation (8.3.7) indicates that t_κ is not a very useful time scale for convection processes, since it is a measure of thermal conduction. A better one would be that given by the second equality in Equation (8.3.7). Thus we can define a time scale characteristic of convection as

$$t_v \equiv (D^2/\kappa)Ra^{-2/3} \tag{8.3.8}$$

To complete this discussion of scaling for now, we will return to the heat flux, estimated in the last section from $q = KT/d$. Using Equation (8.3.3), you can see that

$$q = (KT/D)Ra^{1/3} \tag{8.3.9}$$

Again you can recognise (KT/D) as a scaling quantity. In this case it is the heat that would be conducted across the fluid layer (not the boundary layer) if the base were held at the temperature T and the surface at $T = 0$. In other words, it is the heat that would be conducted in the steady state in the absence of convection. Denote this as q_K. The ratio q/q_K is known as the Nusselt number, denoted as Nu:

$$Nu \equiv q/q_K = qD/KT \tag{8.3.10}$$

Then Equation (8.3.9) reduces to

$$Nu \sim Ra^{1/3} \tag{8.3.11}$$

Thus the Nusselt number is a direct measure of the efficiency of convection as a heat transport mechanism relative to conduction. For the mantle, $Nu \approx 100$. In other words, mantle convection is about two orders of magnitude more efficient at transporting heat than conduction would be.

8.4 Marginal stability

Traditional treatments of convection often begin with an analysis of marginal stability, which is the analysis of a fluid layer just at the point when convection is about to begin. This approach reflects the historical development of the topic, and the fact that the mathematics of marginal stability has yielded analytical solutions. The mantle is far from marginal stability, as we will see, and so I began the topic of convection differently, with the more directly relevant 'finite amplitude' convection problem.

Nevertheless the marginal stability problem gives us some important physical insights into convection and the Rayleigh number. However, many treatments of it give long and intricate mathematical derivations and do not always make the physics clear. I will err in the other direction, keeping the mathematics as simple as possible and endeavouring to clarify the physics.

The marginal stability problem arises from the fact that, for a fluid layer heated uniformly on a lower horizontal boundary, there is a minimum amount of heating below which convection does not occur. If the temperature at the bottom is initially equal to the temperature at the top, then of course there will be no convection. Now if the bottom temperature is slowly increased, still there will

be no convection, until some critical temperature difference is reached, at which point slow convection will begin. At this point, the fluid layer has just become unstable and begins to overturn. The transition, just at the point of instability, is called marginal stability. Lord Rayleigh [3] was the first to provide a mathematical analysis of this. He showed that marginal stability occurs at a critical value of the Rayleigh number. The critical value depends on the particular boundary conditions and other geometric details, but is usually of the order of 1000. The mathematical analysis of marginal stability is reproduced by Chandrasekhar [4] and by Turcotte and Schubert [2] (p. 274).

Consider the two layers of fluid sketched in Figure 8.2. The lower layer is less dense, and the interface between them has a bulge of height h and width w. Take h to be quite small. This bulge is buoyant relative to the overlying fluid, and its buoyancy is approximately

$$B = g\Delta\rho wh$$

per unit length in the third dimension. Its buoyancy will make it grow, so that its highest point rises with some velocity $v = \partial h/\partial t$, and its growth will be resisted by viscous stresses.

The viscous resistance will have different forms, depending on whether the width of the bulge is smaller or larger than the layer depth D. If $w \ll D$, the dominant shear resistance will be proportional to the velocity gradient v/w. The resisting force is then

$$R_s = \mu(v/w)w = \mu v = \mu\partial h/\partial t$$

where v/w is a characteristic strain rate and the subscript 's' denotes small w. Equating B and R_s to balance the forces yields

$$\frac{\partial h}{\partial t} = \frac{g\Delta\rho w}{\mu}h \tag{8.4.1}$$

which has the solution

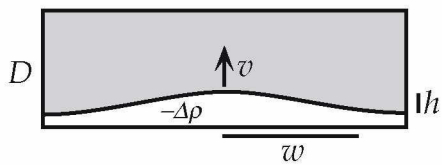

Figure 8.2. Sketch of two layers of fluid with the denser fluid above and with an undulating interface that is unstable.

$$h = h_0 \exp(t/\tau_s) \tag{8.4.2}$$

where h_0 is a constant and

$$\tau_s = \frac{\mu}{g\Delta\rho w} \tag{8.4.3}$$

In other words, the bulge grows exponentially with a time constant τ_s, because the interface is unstable: the lighter fluid wants to rise to the top. This kind of instability is called the Rayleigh–Taylor instability. It occurs regardless of the reason for the density difference between the two fluids.

Notice that τ_s gets smaller as w gets bigger. That is, broader bulges grow more quickly. However, there is a limit to this: when the width of the bulge is comparable to the depth, D, of the fluid layer, the top boundary starts to interfere with the flow and to increase the viscous resistance. If w is much larger than D, then the dominant viscous resistance comes from horizontal shear flow with velocity u along the layer. By conservation of mass, $uD = vw$. The characteristic velocity gradient of this shear flow is then $u/D = vw/D^2$. The resulting shear stress acts across the width w of the bulge, so the resisting force in this case is

$$R_l = \mu(u/D)w = \mu v w^2/D^2$$

where subscript 'l' denotes large w. Balancing R_l and B then yields

$$\frac{\partial h}{\partial t} = \frac{g\Delta\rho D^2}{\mu w} h \tag{8.4.4}$$

which has the same form as Equation (8.4.1) except for the constants. It also has the same form of exponentially growing solution (Equation (8.4.2)), but with a different time scale τ_l:

$$\tau_l = \frac{\mu w}{g\Delta\rho D^2} \tag{8.4.5}$$

Notice here that τ_l gets *bigger* for larger w, whereas τ_s gets smaller, and their values are equal when $w = D$. We have considered the two extreme cases $w \ll D$ and $w \gg D$. As w approaches D from either side, the time scale of the growth of the instability gets smaller. This implies that the time scale is a minimum near $w = D$. In other words, a bulge whose horizontal scale is $w = D$ is the fastest growing bulge, and its growth time scale is

$$\tau_{RT} = \frac{\mu}{g\Delta\rho D} \tag{8.4.6}$$

where the subscript 'RT' connotes the Rayleigh–Taylor time scale. A more rigorous analysis that yields this result is given by Turcotte and Schubert [2] (p. 251). The implication of this result is that if there are random small deviations of the interface from being perfectly horizontal, deviations that have a width comparable to the layer depth will grow exponentially with the shortest time scale and will quickly come to dominate. As a result, the buoyant layer will form into a series of rising blobs with a spacing of about $2w$.

Now let us consider the particular situation in which the density difference is due to the lower layer having a higher temperature because the bottom boundary of the fluid is hot. Then the density difference would be $\Delta\rho = \rho\alpha\Delta T$, where ΔT is a measure of the average difference in temperature between the layers. Suppose first that the thermal conductivity of the fluid is high and the growth of the bulge is negligibly slow: then temperature differences would be quickly smeared out by thermal diffusion. In the process, the bulge would be smeared out. After a time the temperature would approach a uniform gradient between the bottom and top boundaries, and the bulge would have ceased to exist.

However, I showed above that the bulge grows because of its buoyancy. Evidently there is a competition between the buoyancy and the thermal diffusion. We can characterise this competition in terms of the time scales of the two processes: τ_{RT} for the buoyant growth and τ_κ for the thermal diffusion, where

$$\tau_\kappa = D^2/\kappa \tag{8.4.7}$$

We can use D as a measure of the distance that heat must diffuse in order to wipe out the fastest growing bulge. In order for the bulge to grow, τ_{RT} will need to be significantly less than τ_κ. From Equations (8.4.6) and (8.4.7), this condition is

$$\frac{g\Delta\rho D^3}{\kappa\mu} = Ra \geq c \tag{8.4.8}$$

where c is a numerical constant and you can recognise the left-hand side of Equation (8.4.8) as the Rayleigh number.

This result tells us that there is indeed a value of the Rayleigh number that must be exceeded before the thermal boundary layer can rise unstably in the presence of continuous heat loss by thermal diffusion. If it cannot, there will be no thermal convection. Thus we

have derived the essence of Rayleigh's result. In this case, we do not get a very good numerical estimate of the critical value of the Rayleigh number, since a rigorous stability analysis yields $c \approx 1000$, rather than $c \approx 1$.

The quantitative value may not be very accurate, but we have been able to see that the controlling physics is the competition between the Rayleigh–Taylor instability and thermal diffusion (the Rayleigh–Taylor instability involving an ever-changing balance between buoyancy and viscous resistance). In fact, you can see now that the Rayleigh number is just the ratio of the time scales of these two processes:

$$Ra = \frac{\tau_\kappa}{\tau_{\mathrm{RT}}} \tag{8.4.9}$$

The mantle Rayleigh number is at least 3×10^6, well above the critical value of about 1000. This indicates that the mantle is well beyond the regime of marginal stability. One way to look at this, using Equation (8.4.9), is that the thermal diffusion time scale is very long, which means that heat does not diffuse very far in the time it takes the fluid to become unstable and overturn. This means that the thermal boundary layers will be thin compared with the fluid layer thickness.

Thin boundary layers were assumed without comment in the simple theory of convection given in Section 8.2. That theory actually is most appropriate with very thin boundary layers, that is at very high Rayleigh numbers. For this reason it is known as the boundary layer theory of convection. Thus the marginal stability theory applies just above the critical Rayleigh number, while the boundary layer theory applies at the other extreme of high Rayleigh number.

8.5 Flow patterns

In a series of classic experiments, Benard [5] observed that, in a liquid just above marginal stability, the convection flow formed a system of hexagonal cells, like honeycomb, when viewed from above. Considerable mathematical effort was devoted subsequently to trying to explain this. It was presumed that it must imply that hexagonal cells are the most efficient at convecting heat. It turned out that the explanation for the hexagons lay in the effect of surface tension in the experiments, and specifically on differences in surface tension accompanying differences in temperature. Surface tension

was important because Benard's liquid layers were only 1 mm or less in thickness.

There is an important lesson here. If a factor like the temperature-dependence of surface tension could so strongly influence the horizontal pattern, or 'planform', of the convection, then the fluid must not have a strong preference for a particular planform; that is, different planforms must not have much influence on the efficiency of the convection. The implication is that, in other situations, other factors influencing the material properties of the fluid in the boundary layers might also have a strong influence on planform.

Pursuing this logic, if the top and bottom thermal boundary layers in a fluid layer should have material properties that are distinctly different from each other, then each may tend to drive a distinctive pattern of convection. What then will be the resulting behaviour? The possibility of the different thermal boundary layers tending to have different planforms is not made obvious in standard treatments of convection. Whether it occurs depends both on the physical properties of the fluid and on the mode of heating, which we will look at next.

In the mantle, a hot boundary layer does have distinctly different mechanical properties from a cold boundary layer, and the two seem to behave quite differently. As well, the cold boundary layer in the earth is laterally heterogeneous, containing continents and so on, and it develops other heterogeneities in response to deformation: it breaks along faults. The effects of material properties on flow patterns are major themes of the next three chapters, which focus on the particular case of the earth's mantle.

8.6 Heating modes and thermal boundary layers

Textbook examples of convection often show the case of a layer of fluid heated from below and cooled from above. In this case there is a hot thermal boundary layer at the bottom and a cool thermal boundary layer at the top (Figure 8.3a). If, as well, the Rayleigh number is not very high, the resulting pattern of flow is such that each of the thermal boundary layers reinforces the flow driven by the other one. In other words the buoyant upwellings rise between the cool downwellings, so that a series of rotating 'cells' is formed which are driven in the same sense of rotation from both sides. This cooperation between the upwellings and downwellings disguises the fact that the boundary layers are dynamically separate entities. It is possible that they might drive different flow patterns, as I intimated in the last section. It is also possible that one of the thermal boundary layers is weak or absent.

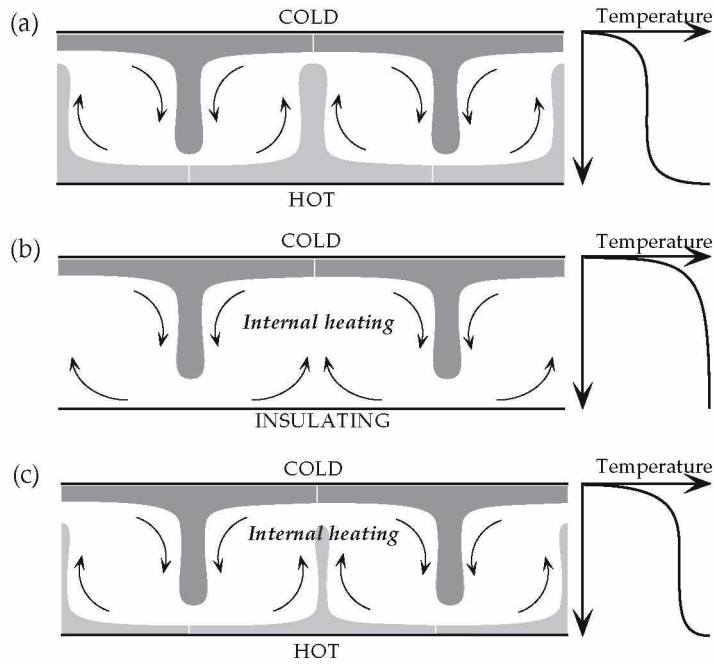

Figure 8.3. Sketches illustrating how the existence and strength of a lower thermal boundary layer depend on the way in which the fluid layer is heated.

For example, a fluid layer might be heated from within by radioactivity. If there is no heat entering the base, perhaps because it is insulating, then there will be no hot thermal boundary at the bottom. If the fluid layer is still cooled from the top, the only thermal boundary layer will be the cool one at the top (Figure 8.3b). In fact this was assumed, without comment, in the simple theory of convection presented in Section 8.2. In this case, the cool fluid sinking from the top boundary layer still drives circulation, but the *upwelling* is *passive*. By this I mean that although the fluid flows upwards between the downwellings (Figure 8.3b), it is not buoyant relative to the well-mixed interior fluid. It is merely being displaced to make way for the actively sinking cold fluid.

Although this may seem to be a trivial point here, it has been very commonly assumed, for example, that because there is clearly upwelling occurring under midocean ridges, the upwelling mantle material is hotter than normal and thus buoyant and 'actively' upwelling. We will see evidence in Chapter 10 that this is usually not true. A lot of confusion about the relationship between mantle convection and continental drift and plate tectonics can be avoided by keeping this simple point clearly in mind.

More generally, the heat input to the fluid layer might be a combination of heat entering from below and heat generated within (by radioactivity, in the case of the mantle), and states intermediate between those of Figures 8.3a and 8.3b will result (Figure 8.3c). Suppose, as implied in Figure 8.3a, that the temperature of the lower boundary is fixed. If there is no internal heating, then the temperature profile will be like that shown to the right of Figure 8.3a. If there is no heating from below, the internal temperature will be the same as the bottom boundary, as shown to the right of Figure 8.3b. If there is some internal heating, then the internal temperature will be intermediate, as in Figure 8.3c. As a result, the top thermal boundary layer will be stronger (having a larger temperature jump across it) and the lower thermal boundary layer will be correspondingly weaker. The mantle seems to be in such an intermediate state, as we will see.

The point is illustrated by numerical models in Figure 8.4. The left three panels are frames from a model with a prescribed bottom temperature and no internal heating. You can see both cool sinking columns and hot rising columns. The right three panels are from an internally heated model, and only the upper boundary layer exists. Downwellings are active, as in the bottom-heated model, but the upwellings are passive, broad and slow. Away from downwellings, isotherms are nearly horizontal, and the fluid is stably stratified. This is because the coolest fluid sinks to the bottom, and is then

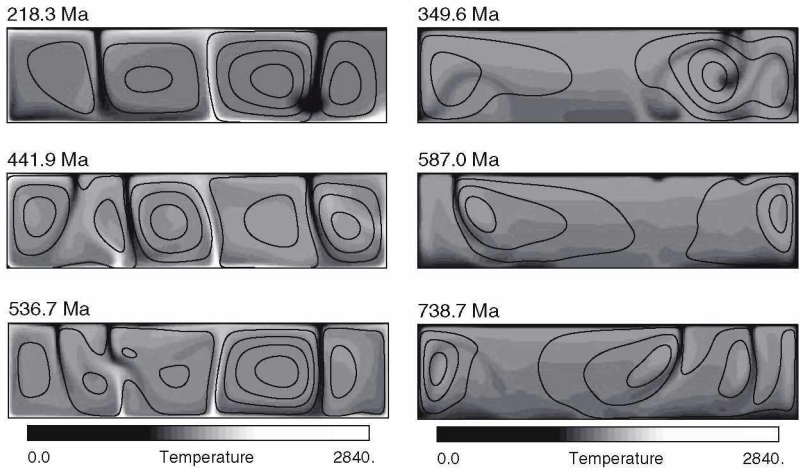

Figure 8.4. Frames from numerical models, illustrating the differences between convection in a layer heated from below (left-hand panels) and in a layer heated internally (right-hand panels). (Technical specifications of these models are given in Appendix 2.)

slowly displaced upwards by later cool fluid as it slowly warms by internal heating.

Figure 8.4 illustrates two other important points. First, the flow is unsteady. This is characteristic of convection at high Rayleigh numbers in constant-viscosity fluids. It is because the heating is so strong that the boundary layers become unstable before they have travelled a distance comparable to the depth of the fluid, which is the width of cells that allows the most vertical limbs while also minimising the viscous dissipation. Incipient instabilities in the top boundary layer are visible in the middle right panel of Figure 8.4. By the last panel they have developed into full downwellings.

Second, the two thermal boundary layers in the left sequence are behaving somewhat independently, especially on the left side of the panels. In fact in the bottom panel an upwelling and a downwelling are colliding. This illustrates the point made earlier that each boundary layer is an independent source of buoyancy, and they may interact only weakly. This becomes more pronounced at higher Rayleigh numbers.

8.6.1 Other Rayleigh numbers [*Advanced*]

We have so far specified the thermal state of the convecting fluid in terms of *temperatures* prescribed for each boundary. However, in Figures 8.3b and 8.4 (right panels) the bottom boundary is specified as *insulating*, that is as having zero heat flux through it, and the heating is specified as being internal. The temperature is not specified ahead of time. It is evident that this model is specified in terms of heat input, rather than in terms of a temperature difference between the boundaries. How then can the Rayleigh number be defined?

The philosophy of the dimensional estimates used in this chapter is that *representative* quantities are used. With appropriate choices, order-of-magnitude estimates will (usually) result. The Rayleigh number defined by Equation (8.3.2) is defined in terms of such representative quantities. This suggests that we look for *representative* and *convenient* measures in different situations.

We lack a representative temperature difference for the situation in Figure 8.3b, but we can assume that a heat flux, q, is specified. One way to proceed is to derive a quantity from q that has the dimensions of temperature; for example, we can use the temperature difference, ΔT_q, across the layer that would be required to *conduct* the specified heat flux, q:

$$\Delta T_q = qD/K$$

We can then define a new Rayleigh number as

$$R_q = \frac{g\rho\alpha D^3 \Delta T_q}{\kappa\mu} = \frac{g\rho\alpha q D^4}{K\kappa\mu} \tag{8.6.1}$$

This Rayleigh number is useful in any situation in which it is the heat input rather than a temperature difference that is specified.

It is possible in principle that some heat, say q_b, is specified at the base, and some is specified to be generated internally. If the internal heating is uniform, and generated at the rate H per unit volume of fluid, then the rate of internal heat generation per unit area of the layer surface is HD. The total heat input will then be

$$q = q_b + HD$$

Although in a laboratory setting it is not easy to prescribe a heat flux, it is easy in numerical experiments and it is useful to make the conceptual distinction between the two kinds of bottom thermal boundary layer: prescribed temperature and prescribed heat flux.

The Rayleigh numbers R_q (Equation (8.6.1)) and Ra (Equation (8.3.2)) are distinct quantities with different numerical values, as we will see, and this is why different symbols are used here for them. However they are also related. Recall that the Nusselt number, Nu, was defined as the ratio of actual heat flux, q, to the heat flux, q_K, that would be conducted with the same temperature difference across the layer (Equation (8.3.10)). In the case considered earlier, it was q_K that was specified ahead of time and q that was determined by the behaviour of the fluid layer. Here it is the reverse. However we can still use this definition of Nu. Thus, if the actual temperature difference across the layer that results from the convection process is ΔT, then $q_K = K\Delta T/D$ and

$$Nu = q/q_K = \Delta T_q/\Delta T \tag{8.6.2}$$

Thus here the Nusselt number gives the ratio of the temperature difference, ΔT_q, that would be required to conduct the heat flux q through the layer, to the actual temperature difference in the presence of convection.

Similarly, although ΔT is not known ahead of time here, it can still be used conceptually to define the Rayleigh number Ra (Equation (8.3.2)). It is then easy to see the relationship between Ra and R_q:

$$\frac{R_q}{Ra} = \frac{\Delta T_q}{\Delta T} = Nu \tag{8.6.3}$$

In the earlier discussion of scaling, we found that $Nu \sim Ra^{1/3}$, so $R_q \sim Ra^{4/3}$. Thus if Ra has the value 3×10^6 estimated earlier, for example, then R_q will be about 4.3×10^8. Thus R_q is numerically larger than Ra. Nevertheless it is a convenient way to characterise cases where it is the heat flux that is specified, rather than the temperature difference. You must of course be careful about which definition of Rayleigh number is being used in a given context, as they have different scaling properties as well as different numerical values.

This discussion illustrates the general point that different Rayleigh numbers may be defined in different contexts. There is nothing profound about this, it is merely a matter of adopting a definition that is convenient and relevant for the context, so that it encapsulates the scaling properties of the particular situation.

For the earth's mantle, however, there is a complication. An appropriate way of specifying the heat input into models of the mantle is through a combination of internal heating from radioactivity and a prescribed temperature at the base. Although the value of the temperature at the base of the mantle is not well known, the liquid core is believed to have a low viscosity, so that it would keep the temperature quite homogeneous. This means the core can be viewed as a heat bath imposing a uniform temperature on the base of the mantle. This combination of a heating rate and a prescribed uniform bottom temperature is not covered by either of the Rayleigh numbers Ra or R_q, so there is not a convenient a priori thermal prescription of mantle models. In the mantle it is the heat *output*, at the top surface that is well-constrained. This means that some trial and error may be necessary to obtain models that match the observed heat output of the mantle.

8.7 Dimensionless equations [*Advanced*]

The equations governing convection are often put into dimensionless form, that is they are expressed in terms of dimensionless variables. This is done to take advantage of the kind of scaling properties that we have been looking at, because one solution can then be scaled to a variety of contexts. There are different ways in which this can be done. We have seen an example of this already, in the different Rayleigh numbers that can be defined, depending on the way the fluid is heated. Other alternatives are more arbitrary. For example, two different time scales are com-

monly invoked, and others are possible. Since these alternatives are not usually presented systematically, I will do so here.

The equations governing the flow of a viscous incompressible fluid were developed in Chapter 6 (Equation (6.6.3)), and the equation governing heat flow with advection, diffusion and internal heat generation was developed in Chapter 7 (Equation (7.8.2)). The following dimensional forms of these equations are convenient here.

$$\frac{\partial \tau_{ij}}{\partial x_j} - \frac{\partial P}{\partial x_i} = -B_i = \rho g_i \tag{8.7.1}$$

$$\frac{\mathrm{D}T}{\mathrm{D}t} \equiv \frac{\partial T}{\partial t} + v_i \frac{\partial T}{\partial x_i} = \kappa \nabla^2 T + \frac{A}{\rho C_P} \tag{8.7.2}$$

In Equation (8.7.1), the buoyancy force B_i (positive upwards), is written in terms of the density and the gravity vector g_i (positive downwards). In Equation (8.7.2), the first derivative, $\mathrm{D}T/\mathrm{D}t$, is known as the total derivative, and its definition is implicit in the first identity of that equation. A is the internal heat production per unit time, per unit volume.

Three scaling quantities suffice to express these equations in dimensionless form: a length, a temperature difference and a time. For length, an appropriate choice is usually D, the depth of the convection fluid layer. Using this, we can define dimensionless position coordinates, x_i, for example, such that

$$x_i' = Dx_i$$

where I have *changed notation*: the prime denotes a dimensional quantity and unprimed quantities are dimensionless, unless specifically identified as a dimensional scaling quantity, like D.

For temperature, we have seen in the last section two possible choices:

$$\Delta T = \Delta T_T = (T_\mathrm{b} - T_\mathrm{s}) \tag{8.7.3}$$

$$\Delta T = \Delta T_q = qD/K \tag{8.7.4}$$

For the moment, I will retain the general notation ΔT to cover both of these possibilities.

A time scale that is often used is the thermal diffusion time scale of Equation (8.3.6): $t_\kappa = D^2/\kappa$. Another one sometimes used is

t_κ/Ra. A third possibility emerged from the earlier discussion of scaling, namely the transit time $t_v = t_\kappa/Ra^{2/3}$ (Equations (8.3.7), (8.3.8)). Here I will carry all three possibilities by using a general time scale t_n, where

$$\begin{aligned} t_1 &= t_\kappa = D^2/\kappa \\ t_2 &= t_\kappa/Ra \\ t_3 &= t_v = t_\kappa/Ra^{2/3} \end{aligned} \tag{8.7.5}$$

Dimensional scales can be derived from D, ΔT and t_n for viscous stress, buoyancy and heat generation rate as follows. Viscous stress is viscosity times velocity gradient, so an appropriate scale is $\mu(D/t_n)/D = \mu/t_n$. Buoyancy per unit volume is $g\Delta\rho = g\rho_0\alpha\Delta T$. Using these scales in Equation (8.7.1) yields

$$\frac{\mu}{Dt_n}\left(\frac{\partial\tau_{ij}}{\partial x_j} - \frac{\partial P}{\partial x_i}\right) = g\Delta\rho(\rho g_i)$$

that is

$$\frac{\partial\tau_{ij}}{\partial x_j} - \frac{\partial P}{\partial x_i} = R_{\mathrm{F}}(\rho g_i) \tag{8.7.6}$$

where R_{F} denotes a dimensionless combination of constants in the force balance equations:

$$R_{\mathrm{F}} = \frac{g\Delta\rho D t_n}{\mu} \tag{8.7.7}$$

Similarly, for Equation (8.7.2) we need a scale for heat generation. The heat flux scale identified earlier (Equations (8.3.9) and (8.3.10)) is q_K, the heat flux that would be conducted with the same temperature difference. The heat generation rate per unit volume that corresponds to this is $q_K/D = K\Delta T/D^2$. Then Equation (8.7.2) becomes

$$\frac{\Delta T}{t_n}\left(\frac{\mathrm{D}T}{\mathrm{D}t}\right) = \frac{\kappa\Delta T}{D^2}\left(\nabla^2 T\right) + \left(\frac{K\Delta T}{\rho C_P D^2}\right)A$$

Remembering that $K/\rho C_P = \kappa$, this can be written

$$\frac{\mathrm{D}T}{\mathrm{D}t} = R_{\mathrm{H}}\left(\nabla^2 T + A\right) \tag{8.7.8}$$

where R_H denotes a dimensionless combination in the heat equation:

$$R_H = \frac{\kappa t_n}{D^2} \tag{8.7.9}$$

Equations (8.7.6) and (8.7.8) are dimensionless versions of the flow and heat equations, and they involve the two dimensionless ratios R_F and R_H. The three choices of time scale proposed in Equations (8.7.5) then yield

$$t_n = t_1 : \qquad R_F = Ra \qquad R_H = 1 \tag{8.7.10a}$$

$$t_n = t_2 : \qquad R_F = 1 \qquad R_H = 1/Ra \tag{8.7.10b}$$

$$t_n = t_3 : \qquad R_F = Ra^{1/3} \quad R_H = 1/Ra^{2/3} \tag{8.7.10c}$$

The choice of time scale is mainly a matter of convenience. With the choice t_3, one dimensionless time unit will correspond approximately with a transit time, regardless of the Rayleigh number, and it will be easier to judge the progress of a numerical calculation. On the other hand, the choice between ΔT_T and ΔT_q depends on the mode of heating of the fluid. The notation thus refers to a more substantial difference in the model than convenience, and more care must be taken to ensure the proper interpretation of results of calculations.

8.8 Topography generated by convection

The topography generated by convection is of crucial importance to understanding mantle convection, since the earth's topography provides some of the most important constraints on mantle convection. Here I present the general principle qualitatively. The particular features of topography to be expected for mantle convection, and their quantification and comparison with observations, will be given in following Chapters. We have already covered one important example in Chapter 7, the subsidence of the sea floor.

The central idea is that buoyancy does two things: it drives convective flow and it vertically deflects the horizontal surfaces of the fluid layer. Because the buoyancy is (in the thermal convection of most interest here) of thermal origin, there are intimate relationships between topography, fluid flow rates and heat transport rates.

The principle is illustrated in Figure 8.5. This shows a fluid layer with three buoyant blobs, labelled (a), (b) and (c). Blob (a) is close to the top surface and has lifted the surface. The surface uplift is required by Newton's laws of motion. If there were no force opposing the buoyancy of the blob, the blob would continuously accelerate. Of course there are viscous stresses opposing the blob locally, but these only shift the problem. The fluid adjacent to the blob opposes the blob, but then this fluid exerts a force on fluid further out. In other words, the viscous stresses *transmit* the force through the fluid, but do not result in any net opposing force. This comes from the deflected surface.

There is, in Figure 8.5, blob (a), a simple force balance: the weight of the topography balances the buoyancy of the blob. Geologists might recognise this as an *isostatic* balance. Another way to think of it is that the topography has negative buoyancy, due to its higher density than the material it has displaced (air or water, in the case of the mantle). Recalling the definition of buoyancy given earlier (Equation (8.1.1)), this implies that the excess mass of the topography equals the mass deficiency of the blob.

As I have already stressed, there is in this very viscous system an *instantaneous* force balance, even though the blob is moving. Such topography has sometimes been referred to as 'dynamic topography', but this terminology may be confusing, because it may suggest that momentum is involved. It is not. The balance is a static (strictly, a quasi-static), instantaneous balance. The 'dynamic' terminology derives from the term 'dynamic stresses', which means the stresses due to the motion, which are the viscous stresses. While this terminology may be technically correct, it is not very helpful, because it may obscure the fact that there is a simple force balance

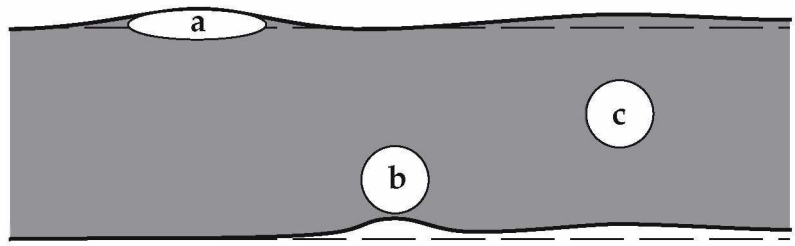

Figure 8.5. Sketch of the effects of buoyant blobs on the surfaces of a fluid layer. The layer surfaces are assumed to be free to deflect vertically, with a less dense fluid (e.g. air or water) above, and a more dense fluid (e.g. the core) below.

involved, and it may make the problem seem more complicated than it really is.

Blob (b) in Figure 8.5 is near the bottom of the fluid layer. It causes the bottom surface of the fluid to deflect. This is because the viscous stresses caused by the blob are larger close to the blob than far away, so the main effect is on the nearby bottom surface. I have implicitly assumed in Figure 8.5 that there is a denser fluid below the bottom surface, such as the core under the mantle. In this case, the topography causes denser (core) material to replace less dense (mantle) material. Thus it generates a downward compensating force, or negative buoyancy, just as does topography on the top surface. This force balances the buoyancy of blob (b).

Does blob (b) cause any deflection of the top surface? Yes, there will be a small deflection over a wide area of the surface. Blob (c) makes this point more explicitly: it is near the middle of the layer, and it deflects both the top and the bottom surfaces by similar amounts. In this case, we can see that the force balance is actually between the positive buoyancy of the blob and the *two* deflected surfaces. In fact this will always be true, even for blobs (a) and (b), but I depicted them close to one surface or the other to simplify the initial discussion, since this makes the deflection of one surface negligible.

To summarise the principle, buoyancy in a fluid layer deflects both the top and the bottom surfaces of the fluid (supposing they are deformable), and the combined weight of the topographies balances the internal buoyancy. The amount of deflection of each surface depends on the magnitude of the viscous stresses transmitted to each surface. This depends on the distance from the buoyancy to the surface. It also depends on the viscosity of the intervening fluid, a point that will be significant in following chapters.

Now apply these ideas to the thermal boundary layers we were considering above. The top thermal boundary layer is cooler and denser than the ambient interior fluid, so it is negatively buoyant and pulls the surfaces down. Because it is adjacent to the top fluid surface, it is this surface that is deflected the most. There will be, to a good approximation, an isostatic balance between the mass excess of the thermal boundary layer and the mass deficiency of the depression it causes. The result is sketched in Figure 8.6 in a form that is like that of the mantle. The topography on the left is highest where the boundary layer is thinnest. Away from this in both directions, the surface is depressed by the thicker boundary layer.

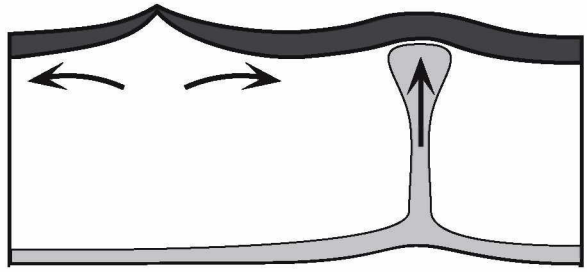

Figure 8.6. Sketch of two types of topography on the top surface of a convecting fluid layer. The top thermal boundary layer cools, thickens and subsides by thermal contraction as it moves away from the spreading centre at left, leaving a topographic high where it is thin. The bottom thermal boundary layer generates no topography on the top surface until material from it rises to the top, where it raises the top surface (upwelling on right).

On the other hand, the bottom thermal boundary layer is adjacent to the bottom surface of the fluid, and generates topography there (Figure 8.6). It does not generate significant topography on the top surface except where a buoyant column has risen to the top of the fluid layer. There the top surface is lifted. Thus it is possible for the bottom thermal boundary layer to generate topography on the top surface, but only after material from it has risen to the top.

There is an important difference between the two topographic highs in Figure 8.6. The high on the left has no 'active' upwelling beneath it: it is high because the surface on either side of it has subsided, because of the negative buoyancy of the top thermal boundary layer. In contrast, the high on the right does have an 'active', positively buoyant upwelling beneath it that has lifted it up.

You will see in the following chapters that the forms of convection driven by the two mantle boundary layers are different. As a result, the forms of topography they generate are recognisably different. Because buoyancy is directly involved both in the topography and in the convection, the observed topography of the earth contains important information about the forms of convection present in the mantle.

Even better, the topography contains *quantitative* information about the fluxes of buoyancy and heat involved. This is most readily brought out in the mantle context, where the topographic forms are distinct and lend themselves to extracting this information. However, it should by now be no surprise to you that such information is present, given the intimate involvement of buoyancy, convection and topography.

8.9 References

1. D. L. Turcotte and E. R. Oxburgh, Finite amplitude convection cells and continental drift, *J. Fluid Mech.* **28**, 29–42, 1967.
2. D. L. Turcotte and G. Schubert, *Geodynamics: Applications of Continuum Physics to Geological Problems*, 450 pp., Wiley, New York, 1982.
3. Lord Rayleigh, On convective currents in a horizontal layer of fluid when the higher temperature is on the under side, *Philos. Mag.* **32**, 529–46, 1916.
4. S. Chandrasekhar, *Hydrodynamic and Hydromagnetic Stability*, Oxford University Press, Oxford, 1961.
5. H. Benard, Les tourbillons cellulaires dans une nappe liquide transportant de la chaleur par convection en régime permanent, *Ann. Chim. Phys.* **23**, 62–144, 1901.

8.10 Exercises

1. Use Equations (8.1.1) and (8.1.2) to evaluate the buoyancy of the following. These are meant to be rough estimates, so do not calculate results to more than one or two significant figures.
   (a) A ball bearing 1 cm in diameter and with density 7.7 Mg/m^3 in mantle of density 3.3 Mg/m^3.
   (b) A plume head with a radius of 500 km and temperature excess of 300 °C in a mantle of density 3.3 Mg/m^3 and thermal expansion coefficient 3×10^{-5}/°C.
   (c) A sheet of subducted lithosphere 100 km thick extending to a depth of (i) 600 km, (ii) 3000 km. Calculate a buoyancy per metre in the horizontal direction of the oceanic trench. Assume the slab temperature varies linearly through its thickness from 0 °C to the mantle temperature of 1300 °C; you need only consider its mean temperature deficit. Assume other parameters as above.
   (d) Suppose part of the slab just considered included oceanic crust 7 km thick with a density in the mantle of 3.2 Mg/m^3. Calculate its contribution to the slab buoyancy.

2. Repeat the derivation of the approximate formula (8.2.5) for the convection velocity in the model of Figure 8.1, but this time assume that the cell length, L, is not the same as its depth, D. You will need to consider the horizontal and vertical velocities, u and v, to be different, and to relate them using conservation of mass. You will also need to include two terms in the viscous resistance, one

proportional to the velocity gradient $2u/D$ and one proportional to $2v/L$. The answer can be expressed in the form of Equation (8.2.5) with the addition of a factor involving (L/D). Using values from the text, compare the velocity when $L = D = 3000\,\text{km}$ and when $L = 14\,000\,\text{km}$, the maximum width of the Pacific plate.